Insight into the Conformational Dynamics of Specific Regions of Porcine Pancreatic Phospholipase A2 from a Time-Resolved Fluorescence Study of a Genetically Inserted Single Tryptophan Residue

Kuipers, Oscar P.; Vincent, Michel; Brochon, Jean-Claude; Verheij, Hubertus M.; Haas, Gerard H. de; Gallay, Jacques

Published in:
Biochemistry

DOI:
10.1021/bi00100a008

Insight into the Conformational Dynamics of Specific Regions of Porcine Pancreatic Phospholipase A_2 from a Time-Resolved Fluorescence Study of a Genetically Inserted Single Tryptophan Residue

Oscar P. Kuipers,[‡] Michel Vincent,[§] Jean-Claude Brochon,[§] Hubertus M. Verheij,[‡] Gerard H. de Haas,[‡] and Jacques Gallay*[,§]

Laboratoire pour l'Utilisation du Rayonnement Electromagnétique, Centre National de la Recherche Scientifique, Ministère de l'Education Nationale, de la Jeunesse et des Sports, Commissariat à l'Energie Atomique, Centre Universitaire Paris-Sud, 91405 Orsay, France, and Department of Biochemistry, Center for Biomembranes and Lipid Enzymology, University of Utrecht, P.O. Box 80054, 3508TB, Utrecht, The Netherlands

Received November 30, 1990; Revised Manuscript Received May 17, 1991

ABSTRACT: The effects of Ca^{2+} and substrate analogue binding on the conformational dynamics of porcine pancreas phospholipase A_2 (PLA_2) in different regions was explored by combining site-directed mutagenesis and time-resolved fluorescence measurements. The single tryptophan residue (Trp-3) of the wild-type protein (W3), in the α-helix A, was replaced by a phenylalanine residue (W3F), whereafter Trp was substituted either for leucine-31 (W31), located in the calcium binding loop, or for phenylalanine-94 (W94), located at the "back side" of the enzyme. Furthermore, mutants lacking the 62–66 sequence were constructed with the Trp at position 3 (ΔW3) or 31 (ΔW31). The total fluorescence intensity decays of Trp in each protein, in the protein–calcium and the protein–calcium–substrate analogue complexes, analyzed by the maximum entropy method (MEM) can be interpreted as distributions of separated lifetime classes. In the case of the W94 mutant, a major short-lived excited-state population ($\tau \sim 50$ ps) is observed, probably deactivated by the interaction with two proximate disulfide bridges via a radiationless process. For the four other mutants, the respective barycenters of the four lifetime classes display comparable values, but the amplitude distributions are different for Trp-3 and Trp-31. The rotational mobility of the Trp residue varies along the peptide chain. Trp-3 experiences only a fast hindered motion. Trp-31 is sensitive to an additional local flexibility that is absent in the N-terminal part of the protein. The largest wobbling angle is observed at position 94. No effect of calcium binding occurs on the lifetime distribution of the Trp-3 and Trp-94 residues. Their mobilities are not affected. In contrast, calcium binding displays a strong influence on the excited-state population distribution of Trp-31. A major population decaying with the longest lifetime is selected in the W31 protein and contributes to ~50% of the decay. The local flexibility and the amplitude of motion of Trp-31 is wider in the protein–calcium complex than in the unliganded protein. Binding of the monomeric substrate analogue *n*-dodecylphosphocholine (C12PN) in the presence of calcium slightly affects the Trp-3 excited-state population distribution and its mobility. Trp-31 is more sensitive to this binding. In particular, a more restricted rotation of the Trp-31 residue and a decrease of the peptide local flexibility as protein–calcium complexes are observed in both the W31 and ΔW31 mutants. The binding of the micellar substrate analogue *n*-hexadecylphosphocholine (C16PN) in the presence of calcium considerably modifies the excited-state population distribution of Trp-3 in the W3 and the ΔW3 proteins. One major broad lifetime population (centered at ~2.6 ns) is selected for the wild-type protein. The internal motion of Trp-3 in both the wild-type and the ΔW3 proteins is strongly reduced. In contrast to these strong effects on position 3, the excited-state population distribution of Trp-31 is only slightly affected by micelle binding as compared to monomer binding. No large changes in the mobility can be observed. The lifetime distribution of Trp-94 is not changed upon micelle binding, but the barycenter value of the major short lifetime is shifted to an even shorter value. The rotational motion is slower and its amplitude is higher in the protein–micelle complex. The results are discussed in terms of specific modulations of the protein structure and flexibility by calcium and substrate analogue binding.

The high sensitivity of the Trp[1] fluorescence emission to the physical and chemical characteristics of its environment (Creed, 1984), has been used extensively to monitor the structural changes that proteins undergo upon, e.g., ligand binding or thermal variations (Beechem & Brand, 1985). The decay rate of tryptophan fluorescence emission is in fact highly sensitive to a variety of factors, including solvation and specific protein structure surrounding the fluorescent residue (Szabo, 1989). Analysis of the excited-state population distribution (Alcala et al., 1987a,b; Livesey & Brochon, 1987; Vincent et al., 1988; Merola et al., 1989; Bajzer et al., 1990; Gentin et

† This work was partially supported by Grant CRE 879015 from the Institut National de la Santé et de la Recherche Médicale (J.G. and M.V.).

* Address correspondence to this author at LURE, Bat 209D, UPS, 91405 Orsay Cedex, France.

‡ University of Utrecht.

§ Centre Universitaire Paris-Sud.

[1] Abbreviations: ACO, anneau de collision d'Orsay; cmc, critical micelle concentration; C12PN, *n*-dodecylphosphocholine; C16PN, *n*-hexadecylphosphocholine; diC6-dithioPC, *rac*-1,2-dihexanoyldithioglycero-3-phosphocholine; diC8-PC, 1,2-dioctanoyl-*sn*-glycero-3-phosphocholine; IRS, interfacial recognition site; NATA, *N*-acetyltryptophanamide; MEM, maximum entropy method; PLA, porcine pancreatic phospholipase A_2 (E.C. 3.1.1.4); Trp, tryptophan; W3, wild-type phospholipase A_2; W3F, wild-type phospholipase A_2 with a Phe at position 3; W31, W3F/L31W PLA_2; W94, W3F/F94W PLA_2; ΔW3, W3 with a 62–66 deletion; ΔW31, W31 with a 62–66 deletion.

0006-2960/91/0430-8771$02.50/0

al., 1990; Siemarczuk et al., 1990; Willis et al., 1990) can provide insight, at the fluorophore level, into the distributions of conformational substrates that are presumed to exist for proteins in solution (Frauenfelder et al., 1988). Furthermore, experiments performed with polarized light can reveal the existence of fast internal rotations and local flexibilities of specific parts of the peptide chain (Munro et al., 1979; Brochon, 1980; Nicot et al., 1985; Datema et al., 1987; Gallay et al., 1987; Petrich et al., 1987; Ludescher et al., 1988; Small & Anderson, 1988; Bucci & Steiner, 1988; Vincent et al., 1988; John & Jähnig, 1988). The technique can describe the functional conformational rearrangements of proteins and can increase our knowledge about the rates of these processes. It can further be used in parallel with theoretical methods (Karplus & McCammon, 1981; McCammon & Harvey, 1987; Sessions et al., 1988) that have been applied to the description of internal fast motions ($\ll$100 ps) in proteins (Henry & Hochstrasser, 1987; McKerell et al., 1988; Axelsen et al., 1988; Axelsen & Prendergast, 1989). Moreover, it offers a direct physical means to measure Brownian rotation of the whole protein and can uncover different rotating species (Wahl, 1983).

As the method is limited to the close environment of the naturally occurring fluorophore, it is tempting to extend its range to other sites inside the molecule. With the availability of genetic engineering, exploration of strategic regions of proteins can now be performed by moving the Trp residue from its natural position to other loci. Amino acids close to the Trp residue in the secondary or tertiary structure can also be modified in order to tentatively ascribe the classes of excited-state lifetimes to specific interactions. The first approach has been applied here to describe the effect of ligand binding at crucial regions of an already well-characterized protein, the porcine pancreatic phospholipase A_2 (PLA_2).

Of all lipolytic enzymes, PLA_2 is probably the most thoroughly characterized protein (Waite, 1987). Already in 1960 its specificity was determined (de Haas et al., 1960), and from then on, a continuing interest in this enzyme has resulted in a detailed, but not at all complete, knowledge of its mode of action [for reviews, see Volwerk and de Haas (1982) and Verheij et al. (1981)]. PLA_2 specifically catalyzes the hydrolysis of the ester bond at the 2-position of 3-*sn*-phosphoglycerides. This reaction is strictly Ca^{2+} dependent and highly stereospecific, since only the natural occurring L-α-phospholipids are degraded by this enzyme. Mammalian pancreas and snakes or bee venoms form a rich source of extracellular PLA_2s, which have a digestive function in the former case and a whole variety of other functions (neurotoxic, anticoagulative, digestive, etc.) in the latter case. The extracellular enzymes are characterized by a molecular mass of about 14 kDa and the presence of six and up to seven disulfide bridges. Up till now, the tridimensional structures of bovine and porcine pancreatic PLA_2s and that of *Crotalus atrox* venom and *Naja naja atra* venom PLA_2s have been determined at 1.7-, 2.6-, 2.5-, and 1.5-Å resolution, respectively (Dijkstra et al., 1981, 1983; Brunie et all., 1985; Scott et al., 1990a), indicating a high degree of structural homology. The crystal structures of complexes with monomeric substrate analogues have also been recently reported (Thunissen et al., 1990; White et al., 1990; Scott et al., 1990b).

Porcine pancreatic PLA_2, which is investigated in this study, displays a low activity on monomeric substrates, which is enhanced by severall orders of magnitude in the presence of lipid–water interfaces. This rate enhancement is the central theme in the study of lipolysis. One of the theories explaining

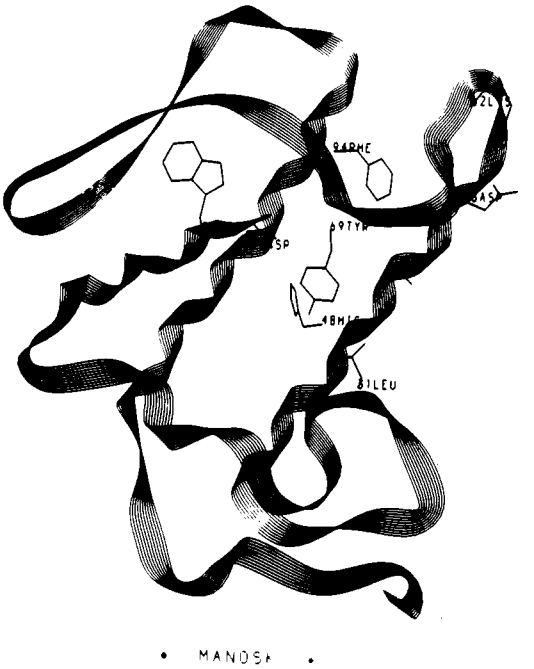

FIGURE 1: Schematic drawing of the tridimensional structure of porcine pancreatic PLA_2. The main chain is represented by a ribbon. The positions of substituted residues in the mutants are indicated in addition to those belonging to the active site. This drawing was performed by use of the graphics program MANOSK (Cherfils et al., 1988).

this considerable increase in enzymatic activity is the IRS model (Volwerk & de Haas, 1982). Briefly, in this model, a single enzyme molecule first binds to the lipid–water interface, which induces a conformational change in the enzyme, resulting in an optimization of the active site and an increase of catalytic rates. Chemical modification, semisynthesis, and site-directed mutagenesis studies (Volwerk & de Haas, 1982; Kuipers et al., 1989a, 1990a) have indicated that residues Leu-2, Trp-3, Arg-6, Leu-19, Met-20, Leu-31, and Tyr-69 in the porcine enzyme are involved in the interaction with lipid–water interfaces. Some of them (i.e., Leu-31 and Tyr-69) are probably also involved in the binding and orientation of a single substrate molecule in the active site (Kuipers et al., 1989a, 1990a; Thunissen et al., 1990). The precise orientation of a phospholipid monomer in the transition state is still unknown, since no tridimensional structure of a complex of PLA_2–Ca^{2+}–micellar substrate analogue has ever been reported.

Among the residues that are involved in the interfacial binding, the single Trp-3 residue deserves attention, since it is the only Trp in the protein and can therefore be used as a structural and dynamic probe. UV-difference absorption spectroscopy studies have indicated a perturbation of the active site residue His-48 and of a Tyr residue upon binding of Ca^{2+} to the enzyme, while the binding of monomers of *n*-decylphosphocholine does not perturb the Trp-3 residue significantly (Pieterson et al., 1974). In addition to the wild-type PLA_2 species, a mutant was produced that contained a deletion of the 62–66 sequence (ΔW3), in the surface loop including residues 60 and 70, located some 10 Å away from Trp-3 (Figure 1). This mutant has been described in a previous publication (Kuipers et al., 1989b). This deletion enhances the enzymatic activity and alters the substrate specificity of the enzyme, and hence, it was of interest whether this surgery would influence the environment and mobility of Trp-3.

The second location for a unique Trp was at position 31 (Figure 1). This residue, which is a Leu in the wild-type

protein, was selected for several reasons. First, it is located at the entrance to the active site and was replaced by Trp, Arg, Ala, Ser, and Gly, respectively, in a recent mutagenesis study (Kuipers et al., 1990a). Only the Trp residue at position 31 increased the affinity of the enzyme for both monomeric and micellar substrate analogues. Second, position 31 is in the middle of the so-called Ca^{2+}-binding loop, which is formed by the carbonyl oxygens of Tyr-28, Gly-30 and Gly-32, and thus provides an excellent opportunity to study the effect of Ca^{2+} binding on the local conformation and flexibility of this loop. It was already known from previous work that the affinity for calcium was not seriously affected by the mutation of the residue at position 31 (Kuipers et al., 1989a). As in the case of the wild-type protein, a mutant containing both the single Trp at position 31 (W3F/L31W) and the deletion (Δ62–66) was constructed, enabling us to study possible local influences of this deletion on the fluorescence of W31.

The third region in the protein that we looked for was an area that was distant from the active site, the Ca^{2+}-binding site, and the IRS. A mutant was constructed with a Phe at position 3 and a Trp at position 94 (W94) (Figure 1).

In this study, the total fluorescence intensity and the anisotropy decays of the single Trp residue of PLA_2 mutants compared to the wild-type protein were measured to get more insight into the local conformational changes occurring when perturbations were brought about at the described specific areas in the protein by ligand binding. A preliminary and partial report of these studies was presented (Kuipers et al., 1990b).

Materials and Methods

Construction and Purification of Mutant Phospholipases. *Escherichia coli* K12 strain PC2494 [Δ(*lac–pro*), *supE*, *thi/F'*, *traD36*, *proA*$^+$*B*$^+$, *lacI*^{q}, *lacZ*ΔM15 (Phabagen collection, Utrecht)] was used for plasmid constructions and as a host for M13-derived vectors. Strain HB2154 (*ara*, Δ(*lac–pro*), *thi/F'*, *proA*$^+$*B*$^+$, *lacI*^{q}, *lacZ*ΔM15, *mutL*::Tn10) was used as a recipient strain in the mutagenesis experiments. Substitutions in the proPLA_2 cDNA, containing several additional restriction sites, were introduced by the gapped duplex procedure, with use of amber selection. The following were used as mutagenic primers for site-directed mutagenesis:

W3F: 5'T AAT CAT GCT T*CG AAA CTG A*A*A TAA TGC CC 3'

L31W: 5'C TGA TCC ACC C*C*A* GCC ACA GTA G 3'

F94W: 5' CAG TTA CAG ATC* C*AT* GCC TCA CAA G 3'

Δ62–66: 5'GCT TTC GGT GTA GGG ATA* Δ ACA GCC* T*G*A* CAG GTT CTT GGC ATC TC 3'

The sites of mutation in the sequence of the oligonucleotides, which were synthesized on a Biosearch 6800 DNA synthesizer, are denoted by an asterisk. The resulting mutant proPLA_2 cDNA was sequenced by the dideoxy chain termination method after plaque purifying. First, mutant W3F was constructed by ligating the *Bam*HI–*Kpn*I fragment from M13, coding from the W3F mutation, into the expression vector pOK13, yielding pOK13W3F. Subsequently, either the mutation L31W was applied by site-directed mutagenesis of M13W3F with the oligonucleotide coding for L31W and subsequent cloning of the M13 *Bam*HI–*Kpn*I fragment into expression vector pOK13, yielding the double mutant pOK13W3F/L31W, or the mutation F94W was applied by cloning the *Stu*I–*Bgl*II fragment of the M13 F94W mutant into pOK13W3F, yielding the double mutant pOK13W3F/F94W. Mutant ΔW3F/L31W was obtained by cloning the *Kpn*I–*Bgl*II fragment of M13 Δ62–66 DNA into pOK13W3F/L31W, and mutant Δ62–66 was obtained as described previously (Kuipers et al., 1989b). After transformation and expression in *E. coli* K12 strain MC4100, containing plasmid pCI857, the mutant phospholipases were obtained by tryptic cleavage of reoxidized fusion protein and purified by CM-cellulose chromatography at pH 5 and 6. Final purification to homogeneity was achieved on DEAE-cellulose at pH 8.5.

Phospholipids. DiC8-PC was obtained after reacylation of *sn*-glycero-3-phosphocholine. DiC6-dithioPC was obtained as described by Volwerk et al. (1979). C12PN and C16PN were synthesized as described previously (Van Dam-Mierras et al., 1975).

Enzymatic Assays. Quantitative measurements with diC8-PC as a substrate were carried out with a titrimetric assay at pH 8 in the presence of 1 mM borate, 25 mM $CaCl_2$, and 100 mM NaCl at 25 °C. The buret of the Radiometer ABU was filled with 10 mM sodium hydroxide. Activities on monomeric diC6-dithioPC were determined at pH 8 in the presence of 200 mM Tris, 100 mM NaCl, and 100 mM $CaCl_2$, as described previously (Volwerk et al., 1979).

Direct Binding of PLA_2 to Monomers and Micelles. The affinities of PLA_2 for monomeric and micellar substrates were determined by following the increase of tyrosine and tryptophan fluorescence upon addition of increasing concentrations of the nonhydrolyzable substrate analogues C12PN (cmc = 1.3 mM) for monomer binding and C16PN (cmc = 10 μM) for micelle binding. Spectra were recorded at 25 °C with a Perkin-Elmer LS-5 luminescence spectrometer. The excitation was performed at 280 nm and the emission spectra were recorded from 310 to 370 nm with 5-nm bandwidth. Assays were performed in buffer containing 100 mM sodium acetate, 50 mM $CaCl_2$, and 100 mM NaCl at pH 6.0. Protein concentrations were 7–8 μM. From saturation curves obtained with lipid monomers, a K_d value can directly be calculated. The data concerning protein–micellar substrate interactions were analyzed in terms of the binding of the enzyme to a theoretical lipid particle consisting of N monomers with a dissociation constant K_d. As has been extensively discussed by de Araujo et al. (1979), the NK_d value is the experimental concentration at which 50% of the enzyme is saturated with micelles.

Fluorescence Measurements. All proteins were dissolved in a buffer containing 100 mM sodium acetate, 100 mM NaCl, and 1 mM EDTA, pH 6.0. Stock solutions of 1 M $CaCl_2$, 100 mM C12PN, and 40 mM C16PN were also made in this buffer. Final concentrations of the ligands used in these studies were 50 mM for Ca^{2+}, 0.8 mM for C12PN, and 4 mM for C16PN. Optical density of protein at 300 nm was ~0.05.

Fluorescence emission spectra were recorded at 21 °C on a modified SLM 8000 spectrofluorometer, interfaced to a Macintosh SE microcomputer. The emission polarizer was set at 55° from the vertically oriented excitation polarizer. Correction for the polarization bias was performed with an unpolarized sample (NATA in buffer at 21 °C).

Steady-state fluorescence anisotropy was measured at 21 °C on the same spectrofluorometer in the T-format mode. Excitation wavelength was set at 300 nm (1-nm bandwidth), and the fluorescence emission was collected through a cutoff filter ($CuSO_4$ 1 M, 2-cm optical path).

Total fluorescence and anisotropy decays were obtained from the polarized components $I_{vv}(t)$ and $I_{vh}(t)$ on either of the two experimental setups on the synchrotron radiation

machine Super-ACO (SA1 or SB1 windows). The storage ring provides a light pulse with a full width at half-maximum (FWHM) of ~500 ps at a frequency of 8.33 MHz for a double bunch mode. The excitation wavelength was set at 300 nm (bandwidth 5 nm) except for the W94 protein for which the excitation wavelength was set at 295 nm. The emission wavelength was set at 350 nm (bandwidth 6 or 10 nm). In most of the experiments a Hammamatsu microchannel plate R1564U-06 was utilized, whereas in a few of them a XP2020Q phototube was used. Data for $I_{vv}(t)$ and $I_{vh}(t)$ were stored in separate memories of a plug-in multichannel analyzer card (Canberra) in a DESKPRO 286E microcomputer (Compaq). Cumulation was stopped when 10^5 to 2×10^5 counts were stored in the peak channel for the total fluorescence intensity decay. The instrumental response function was automatically monitored in alternation with the parallel and perpendicular components of the polarized fluorescence decay by measuring the sample-scattering light at the emission wavelength. The automatic sampling of the data was driven by the microcomputer.

Data Analysis of the Total Intensity Decay. Data analysis of the total intensity decay was performed by the maximum entropy method (Livesey & Brochon, 1987) with use of MEMSYS2 as a library of subroutines (MEDC Ltd., U.K.).

The principles of MEM as applied to time-resolved fluorescence are outlined below. With a vertically polarized light, the parallel $I_{vv}(t)$ and perpendicular $I_{vh}(t)$ components of the fluorescence intensity at time t after the start of the excitation are

$$I_{vv}(t) = \frac{1}{3}E_\lambda(t)^* \int_0^\infty \int_0^\infty \int_{-0.2}^{0.4} \gamma(\tau,\theta,A)\, e^{-t/\tau}(1 + 2Ae^{-t/\theta})\mathrm{d}\tau\, \mathrm{d}\theta\, \mathrm{d}A \quad (1)$$

and

$$I_{vh}(t) = \frac{1}{3}E_\lambda(t)^* \int_0^\infty \int_0^\infty \int_{-0.2}^{0.4} \gamma(\tau,\theta,A)\, e^{-t/\tau}(1 - Ae^{-t/\theta})\mathrm{d}\tau\, \mathrm{d}\theta\, \mathrm{d}A \quad (2)$$

where $E_\lambda(t)$ is the temporal shape of the excitation flash, * denotes a convolution product, and $\gamma(\tau,\theta,A)$ represents the number of fluorophores with fluorescence lifetime τ, rotational correlation time θ, and initial anisotropy A.

If we are only interested in the determination of the total intensity decay parameters, we can considerably simplify the analysis by summing the parallel and perpendicular components:

$$T(t) = I_{vv}(t) + 2I_{vh}(t) = E_\lambda(t)^* \int_0^\infty \alpha(\tau)e^{-t/\tau}\mathrm{d}\tau \quad (3)$$

$\alpha(\tau)$ is the lifetime distribution given by

$$\alpha(\tau) = \int_0^\infty \int_{-0.2}^{0.4} \gamma(\tau,\theta,A)\, \mathrm{d}\theta\, \mathrm{d}A \quad (4)$$

In order to ensure our recovered distribution agrees with our data, we maximize S (Jaynes, 1983; Livesey & Skilling, 1985):

$$S = \int_0^\infty \alpha(\tau) - m(\tau) - \alpha(\tau) \log \frac{\alpha(\tau)}{m(\tau)}\, \mathrm{d}\tau \quad (5)$$

where $m(\tau)$ is the starting lifetime distribution flat in log τ space and $\alpha(\tau)$ is the resulting distribution.

S was subjected to the following constraint:

$$\sum_{k=1}^{M} \frac{(T_k^{calc} - T_k^{obs})^2}{\sigma^2{}_k} \leq M \quad (6)$$

where T_k^{calc} and T_k^{obs} are the kth calculated and observed intensities. $\sigma^2{}_k$ is the variance of the kth point ($\sigma^2{}_k = \sigma^2{}_{k,vv} + 4G_{corr}{}^2\sigma^2{}_{k,vh}$; Wahl, 1979). M is the total number of observations and G_{corr} is a factor compensating for the difference in transmission by the emission monochromator of the parallel and perpendicular light.

The center τ_j of a single class j of lifetimes over the $\alpha(\tau_i)$ distribution is defined as

$$\tau_j = \sum_i \alpha(\tau_i)\tau_i / \sum_i \alpha(\tau_i) \quad (7)$$

the summation being performed on the significant values of the $\alpha_i(\tau_i)$ for the j class. C_i is the normalized contribution of the lifetime class j. A lifetime domain spanning 150 values equally spaced on a logarithmic scale between 0.1 and 20.0 ns was routinely used in the analyses.

Fluorescence Anisotropy Decay Analysis and Interpretation. Data analysis of

$$R(t) = [I_{vv}(t) - G_{corr}I_{vh}(t)]/[i_{vv}(t) + 2G_{corr}I_{vh}(t)] \quad (8)$$

was performed by nonlinear least-squares regression (Wahl, 1979). The decays were fitted to the expression

$$A(t) = \sum_j \beta_j \exp(-t/\theta_j) \qquad \text{with } 2 \leq j \leq 3 \quad (9)$$

where β_j is the contribution to the anisotropy of the rotational correlation time θ_j. In this analysis, we postulate that each excited-state population undergoes the same rotational motions, then $A(t) = R(t)$.

In some cases, $\Sigma\beta_j$ was smaller than A_0, the intrinsic anisotropy value measured in vitrified medium (for Trp excited at 295 and 300 nm, $A_0 = 0.220$ and 0.300 respectively; Valeur & Weber, 1977). This indicates the occurrence of a very fast motion, undetectable owing to the present time resolution of the experimental setup.

For a residue in a protein, the internal rotation is restricted (Ichiye & Karplus, 1983). The semiangle of the cone (ω_{max}) of the free rotation in the subnanosecond time scale of the fluorophore transition dipole was calculated by use of published expressions (Kinosita et al., 1977; Lipari & Szabo, 1980):

$$\sum_j \beta_j / A_0 = [(\cos \omega_{max})(1 + \cos \omega_{max})/2]^2 \qquad \text{with } j \neq 1 \quad (10)$$

The application of such a model to the Trp motion inside a protein is only for the sake of comparison, since the geometry of the motion remains unknown.

The overall correlation of the protein as a whole rotating body can be described simply in an equivalent sphere approximation model as

$$\theta = V_h\eta/kT \quad (11)$$

where V_h is the hydrated volume of the particle, η is the solvent viscosity, and T is the temperature. From the correlation time value, the hydrated volume and the Stokes' radius values can be calculated.

Results

Kinetic Characterization of the PLA_2 Mutants. Our purpose has been to produce single Trp containing mutants of porcine pancreatic PLA_2 that have properties that make them well suited for ligand binding studies by time-resolved fluorescence.

To test the ligand binding of the mutant enzymes, several kinetic assays and direct binding studies have been performed. It was already known from previous studies that the affinity

Table I: Kinetic Constants for the Hydrolysis for the Monomeric Substrate diC6-dithioPC and Binding Constants for the Substrate Analogue C12PN Monomer of the Wild-Type and Five Mutant Phospholipases A_2

	diC6-dithioPC			
enzyme	$k_{cat}(s^{-1})$	K_M (mM)	k_{cat}/K_M (s^1 M^1)	C12PN K_d (mM)
wild type (W3)	0.72[a]	0.80	900	0.3
Δ62–66 (ΔW3)	0.88	0.50	1760	0.8
W3F/L31W (W31)	0.51	0.32	1590	0.05
ΔW3F/L31W (ΔW31)	0.57	0.17	3350	0.04
W3F/F94W (W94)	0.70	0.85	820	nd[b]
W3F	0.69	0.83	830	nd

[a] Standard errors were about 10% for each given value. [b] nd: not determined because the rise in fluorescence signal was too low.

Table II: Kinetic Constants for the Hydrolysis of the Micellar Substrate diC8-PC and Binding Constants for the Micellar Substrate Analogue C16PN for the Wild-Type and Five Mutant Phospholipases A_2

	diC8-PC		
enzyme	V_{max} (mmol min^{-1} mg^{-1})	K_M^{app} (mM)	C16PN NK_d (μM)
wild type (W3)	2000	3.7	70
Δ62–66 (ΔW3)	4300	2.8	140
W3F/L31W (W31)	320	5.9	230
ΔW3F/L31W (ΔW31)	860	6.1	300
W3F/F94W (W94)	260	22.1	nd[a]
W3F	330	15.7	nd

[a] nd: not determined because the rise in fluorescence signal was too low.

for calcium ions was hardly affected by mutations at position 3 and 31. The K_{Ca}^{2+} values for the corresponding proteins are about 2.2 ± 0.6 mM and are well below the 50 mM concentration we used in this study. Residue 94 is located far away from the calcium ion in the tridimensional structure (Dijkstra et al., 1983), and therefore it was highly unlikely that there will be any effect of the F94W mutation on the calcium binding, compared to that of the wild-type enzyme.

In Table I, the results of the kinetic studies with monomeric diC6-dithioPC are listed as well as that of the direct binding studies with monomeric C12PN. The results make clear that all mutants retain considerable enzymatic activities and substrate affinity, which enables us to monitor the effects of monomer binding in the time-resolved fluorescence studies.

Table II summarizes the results of kinetic studies with the micellar substrate diC8-PC and of the binding studies with the micellar substrate analogue C16PN. Although most mutants display reduced V_{max} values on this substrate, these data show that we still have biologically active enzymes. The affinities for micelles are somewhat reduced for the mutant PLA_2's, but in any case, the NK_d values for C16PN make saturating the 4 mM concentration used in this study. Only for the W94 mutant, a considerable loss of affinity for C16PN micelles occurs. By extrapolation from the kinetic data on diC8-PC, one could estimate an upper limit of 1 mM for the NK_d value, which is still 4 times below the concentration we used in this study. Results with mutant W3F are included to show the effect of this mutation on the ligand binding properties but were not used in the fluorescence study.

Total Fluorescence Emission Parameters of the PLA_2 Mutants. The fluorescence spectra of the PLA_2 derivatives with a single Trp residue at different positions along the peptide chain exhibit maxima around 346–355 nm when excited at 300 nm (Table III). As a comparison, the emission maximum of NATA in aqueous solution occurs at 355 nm on the same instrument. The 62–66 deletion does not affect the

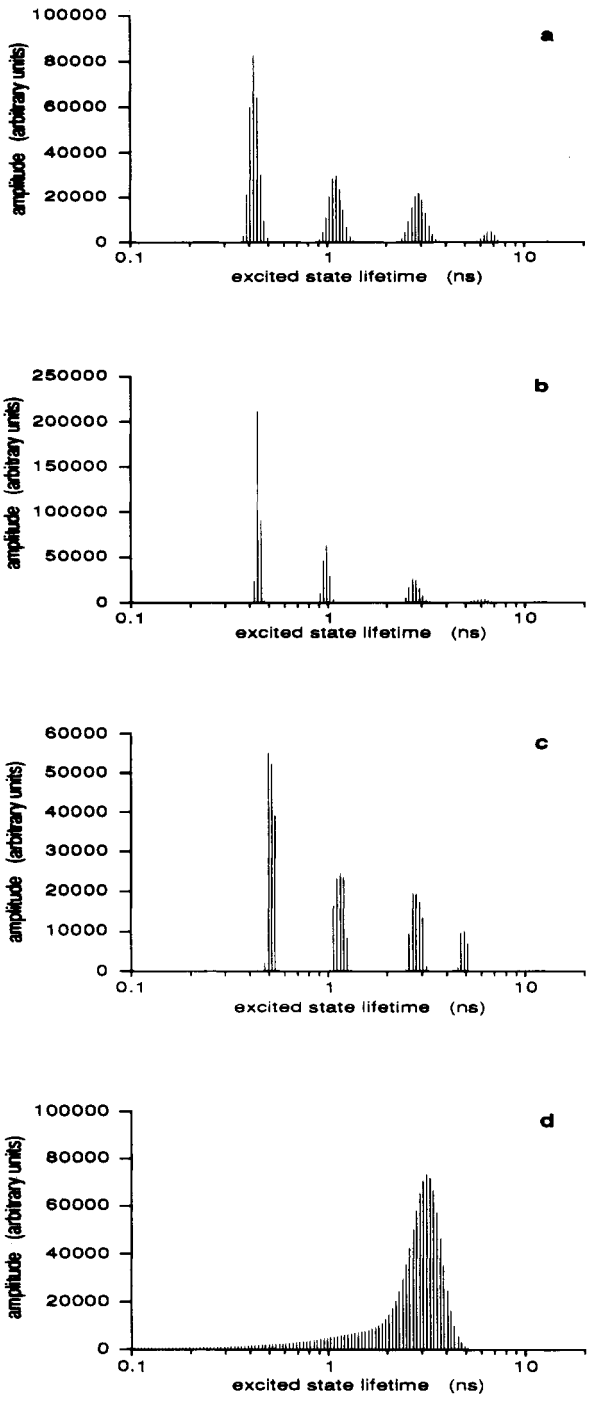

FIGURE 2: MEM-recovered excited-state lifetime distribution of the wild-type PLA_2 protein (W3): (a) unliganded protein; (b) protein in the presence of 50 mM $CaCl_2$; (c) protein in the presence of 50 mM $CaCl_2$ and 0.8 mM C12PN (monomeric form of the substrate analogue); (d) protein in the presence of 50 mM $CaCl_2$ and 4 mM C16PN (micellar form of the substrate analogue). The experimental conditions are described under Materials and Methods.

Trp-3 quantum yield but decreases that of Trp-31. In any case, Trp-31 displays a higher quantum yield value than Trp-3. The W94 mutant displays a very low quantum yield value.

For all these single Trp containing proteins, the total intensity decays are described by a discrete series of exponentials with MEM analysis. Results obtained for all the mutants are presented in Table IV. Four lifetime classes are resolved for the emission of the Trp at position 3 in the wild-type protein (Figure 2). The longest component, however, contributes only to a minor extent to the decay but is systematically found. The lifetime distribution pattern is not significantly modified by

Table III: Steady-State Fluorescence Intensity Parameters of the PLA_2 Mutants: Effect of Calcium Binding

	λ_{max} (nm)		quantum yield[a]	
enzyme	no Ca^{2+}	50 mM Ca^{2+}	no Ca^{2+}	50 mM Ca^{2+}
W3	348	348	0.07	0.07
ΔW3	348	344	0.07	0.07
W31	348	352	0.13	0.18
ΔW31	355	355	0.11	0.13
W94	346	346	0.001	0.001

[a] Quantum yields (QY) have been calculated relative to NATA by assuming a value of 0.14 in buffer (Werner & Forster, 1979). Excitation wavelength was 300 nm.

the 62–66 deletion (Figure 3). When the Trp residue is located at position 31, four lifetime classes are also found by MEM (Figure 4). The deletion of the 62–66 loop decreases the contribution of the shortest lifetime (Figure 5). One can remark that, within the experimental error, the barycenter of the respective lifetime classes shows very similar values in these four mutants, especially for the three shortest values. The mean values calculated for the four mutants are 0.49 ± 0.08 ns, 1.50 ± 0.14 ns, 3.33 ± 0.20 ns, and 6.66 ± 1.5 ns. However, the relative contributions of the long lifetimes are higher in the W31 mutants than in the W3 proteins.

The W94 mutant exhibits only three lifetime families, and the decay is dominated by a short time component in agreement with the low quantum yield value (Figure 6).

Rotational Behavior of the Trp Residue as a Function of Its Position along the Peptide Chain. Time-resolved fluorescence anisotropy decay measurements reveal large differences in the rotational motion of the Trp residue depending on its position (Tables V and VI). In the case of Trp-3, only a single long correlation time could be determined in most of the experiments (Table V). In some measurements, a fast correlation time of ~100 ps was detected. The initial anisotropy value is significantly lower than the expected one of 0.3 generally met for Trp in proteins when excited at 300 nm. The amplitude of the fast motion is not very large, and the calculated wobbling angle value (Kinosita et al., 1977) is low (Table V). The 62–66 deletion does not exert any significant effect either on the Trp-3 dynamics or on the overall protein rotation (Table V).

The fluorescence anisotropy decay of Trp-31 can be described by a sum of two or three exponentials (Table VI). The triple-exponential model improved slightly the χ^2 value as compared to the biexponential model. The initial anisotropy value was increased to some extent. In addition to the fast motions of the indole ring, which are not fully resolved in these

Table IV: Effects of Ligand Binding on the Total Intensity Decay Parameters of the Wild-Type and of the Mutants of PLA_2[a]

	c_1	c_2	c_3	c_4	τ_1 (ns)	τ_2 (ns)	τ_3 (ns)	τ_4 (ns)	$\langle\tau\rangle$
W3	0.49 ± 0.05	0.24 ± 0.05	0.23 ± 0.04	0.04 ± 0.02	0.49 ± 0.10	1.30 ± 0.31	3.10 ± 0.37	7.11 ± 0.93	1.55
+Ca^{2+}	0.54 ± 0.06	0.22 ± 0.04	0.22 ± 0.05	0.03 ± 0.01	0.52 ± 0.06	1.27 ± 0.20	3.10 ± 0.22	7.48 ± 0.99	1.47
+Ca^{2+} + C12PN (mono)	0.41 ± 0.02	0.22 ± 0.08	0.28 ± 0.07	0.10 ± 0.03	0.57 ± 0.08	1.19 ± 0.06	2.71 ± 0.13	4.73 ± 0.21	1.73
+Ca^{2+} + C12PN (micelle)		0.25	0.66	0.09		0.99	2.56	4.34	2.33
+C16PN (micelle)			1				2.57		2.57
ΔW3	0.54 ± 0.10	0.21 ± 0.09	0.22 ± 0.12	0.03 ± 0.02	0.60 ± 0.07	1.50 ± 0.05	3.18 ± 0.47	7.48 ± 1.11	1.68
+Ca^{2+}	0.71 ± 0.06	0.18 ± 0.02	0.10 ± 0.04	0.01 ± 0.00	0.71 ± 0.03	1.67 ± 0.05	3.58 ± 0.93	8.60 ± 0.60	1.25
+Ca^{2+} + C12PN (mono)	0.50 ± 0.02	0.23 ± 0.03	0.22 ± 0.01	0.06 ± 0.04	0.77 ± 0.03	1.37 ± 0.17	3.11 ± 0.43	5.60 ± 0.74	1.72
+Ca^{2+} + C12PN (micelle)	0.12 ± 0.10	0.45 ± 0.11	0.43 ± 0.21		0.82 ± 0.04	1.74 ± 0.39	3.06 ± 0.22		2.20
+Ca^{2+} + C16PN (micelle)		0.28 ± 0.03	0.72 ± 0.04			1.06 ± 0.24	2.67 ± 0.22		2.22
W31	0.23 ± 0.02	0.33 ± 0.01	0.30 ± 0.03	0.13 ± 0.03	0.47 ± 0.14	1.63 ± 0.15	3.36 ± 0.14	5.66 ± 0.17	2.39
+Ca^{2+}	0.10 ± 0.02	0.10 ± 0.04	0.30 ± 0.04	0.50 ± 0.01	0.22 ± 0.09	1.18 ± 0.14	3.25 ± 0.44	5.53 ± 0.12	3.88
+Ca^{2+} + C12PN (mono)	0.10 ± 0.04		0.17 ± 0.03	0.73 ± 0.06	0.47 ± 0.19		2.49 ± 0.28	5.88 ± 0.22	4.76
+Ca^{2+} + C12PN (micelle)		0.09	0.27	0.64		1.17	2.79	5.00	4.06
+Ca^{2+} + C16PN (micelle)		0.11 ± 0.01	0.30 ± 0.02	0.59 ± 0.03		0.89 ± 0.12	2.73 ± 0.21	5.29 ± 0.09	4.04
ΔW31	0.14 ± 0.04	0.30 ± 0.02	0.40 ± 0.02	0.16 ± 0.02	0.41 ± 0.01	1.56 ± 0.06	3.28 ± 0.01	5.29 ± 0.02	2.68
+Ca^{2+}			0.17 ± 0.07	0.82 ± 0.07			2.07 ± 0.35	4.32 ± 0.19	3.89
+Ca^{2+} + C12PN (mono)	0.12 ± 0.06		0.30 ± 0.13	0.58 ± 0.08	0.52 ± 0.25		2.60 ± 0.15	4.26 ± 0.16	3.31
+Ca^{2+} + C12PN (micelle)		0.07	0.11	0.82		0.83	1.89	4.92	4.30
+Ca^{2+} + C16PN (micelle)		0.16 ± 0.01	0.32 ± 0.04	0.53 ± 0.02		0.71 ± 0.00	3.41 ± 0.06	5.67 ± 0.04	4.21
W94	0.94 ± 0.01	0.05 ± 0.02	0.01 ± 0.01		0.05 ± 0.02	0.78 ± 0.21	3.28 ± 0.69		0.12
+Ca^{2+}	0.93 ± 0.02	0.06 ± 0.02	0.02 ± 0.01		0.08 ± 0.04	0.84 ± 0.04	3.36 ± 0.19		0.19
+Ca^{2+} + C16PN (micelle)	0.94 ± 0.03	0.04 ± 0.02	0.01 ± 0.01		0.04 ± 0.01	0.61 ± 0.11	3.10 ± 0.23		0.09

[a] The total intensity decay was assumed as $T(t)\sum_{i=1}^{150}\alpha_i \exp(-t/\tau_i)$. τ_j values are the barycenters of the lifetime class j and c_j values are the normalized areas over each class. $\langle\tau\rangle$ was calculated from $\sum c_j\tau_j/\sum c_j$. ± denotes standard deviations from three up to seven experiments.

Table V: Effects of Ligand Binding on the Anisotropy Parameters of Trp-3 and Trp-94 in PLA_2 Protein Derivatives[a]

enzyme	β_1	β_2	θ_1 (ns)	θ_2 (ns)	θ_{max}
W3		0.221 ± 0.022		7.7 ± 0.7	26
+Ca^{2+}		0.214 ± 0.010		7.2 ± 0.4	27
+C12PN (mono)	0.023 ± 0.003	0.188 ± 0.001	0.14 ± 0.04	7.8 ± 0.1	31
+C12PN (micelle)	0.084	0.237	0.04	15.9	22
+C16PN (micelle)	0.030 ± 0.001	0.273 ± 0.001	0.23 ± 0.04	28.5 ± 0.1	14
ΔW3		0.225 ± 0.006		7.2 ± 0.5	25
+Ca^{2+}		0.218 ± 0.009		7.9 ± 0.1	26
+C12PN (mono)		0.205 ± 0.004		8.3 ± 0.6	28
+C12PN (micelle)	0.031 ± 0.024	0.239 ± 0.007	0.16 ± 0.09	14.6 ± 0.4	22
+C16PN (micelle)	0.048 ± 0.016	0.265 ± 0.004	0.15 ± 0.05	23.6 ± 0.6	16
W94*	0.132 ± 0.021	0.113 ± 0.036	0.57 ± 0.30	7.5 ± 1.9	44
+C16PN (micelle)	0.130 ± 0.005	0.081 ± 0.003	1.74 ± 0.03	24.9 ± 0.4	51

[a] The anisotropy decay was assumed as a sum of exponentials: $r(t) = \sum\beta_i \exp(-t/\theta_i)$. θ_{max} was calculated according to Kinosita et al. (1977). Excitation wavelength was 300 nm except for that of the asterisked entry (295 nm). Emission wavelength: 350 nm.

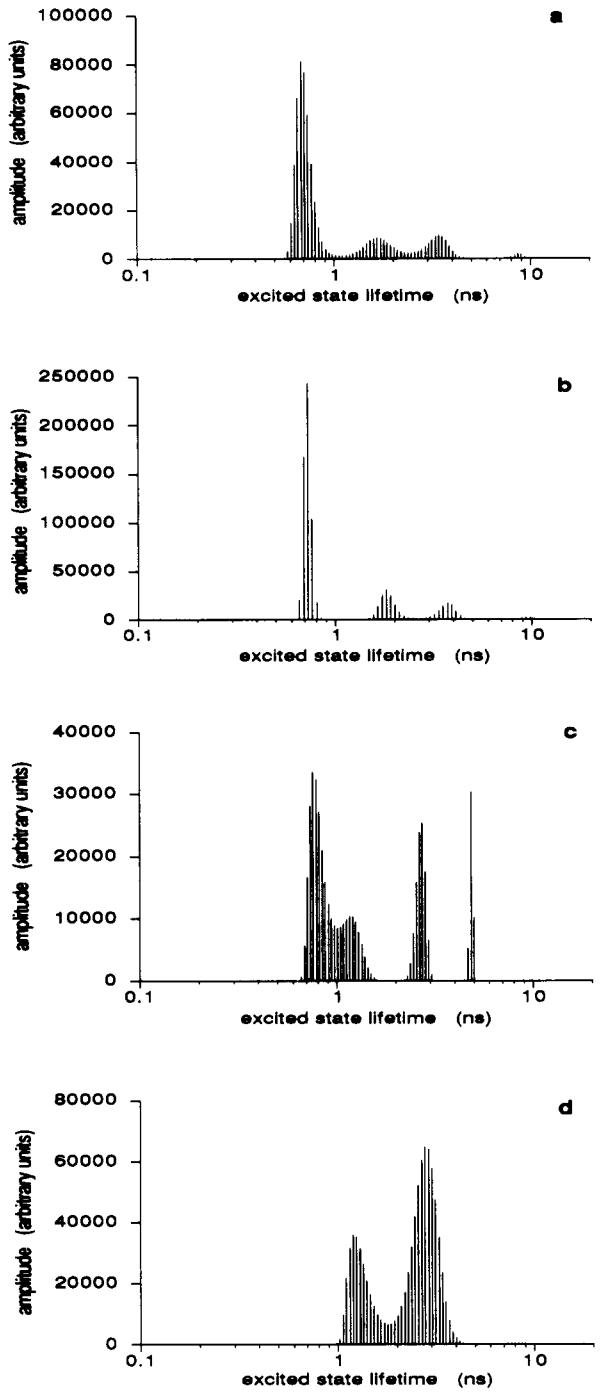

FIGURE 3: MEM-recovered excited-state lifetime distribution of the ΔW3 PLA_2 mutant: (a) unliganded protein; (b) protein in the presence of 50 mM $CaCl_2$; (c) protein in the presence of 50 mM $CaCl_2$ and 0.8 mM C12PN (monomeric form of the substrate analogue); (d) protein in the presence of 50 mM $CaCl_2$ and 4 mM C16PN (micellar form of the substrate analogue). The experimental conditions are described under Materials and Methods.

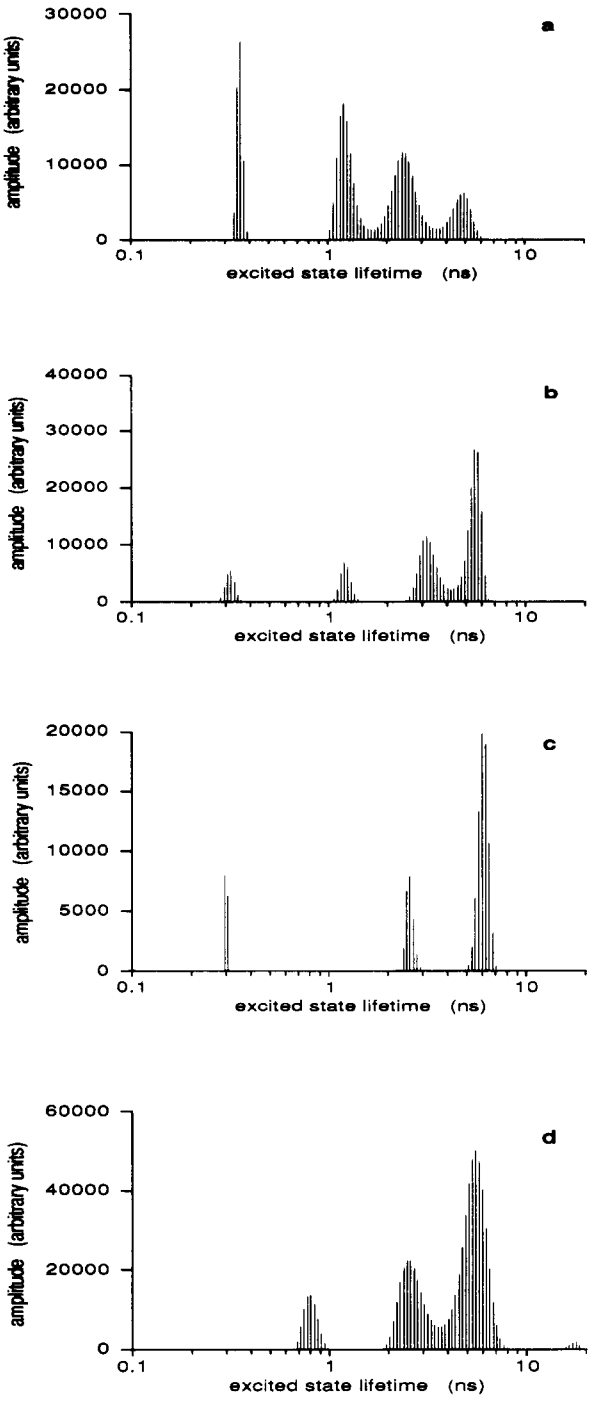

FIGURE 4: MEM-recovered excited-state lifetime distribution of the W31 PLA_2 mutant: (a) unliganded protein; (b) protein in the presence of 50 mM $CaCl_2$; (c) protein in the presence of 50 mM $CaCl_2$ and 0.8 mM C12PN (monomeric form of the substrate analogue); (d) protein in the presence of 50 mM $CaCl_2$ and 4 mM C16PN (micellar form of the substrate analogue). The experimental conditions are described under Materials and Methods.

measurements, a flexibility characterized by a correlation time of ~1 ns, which was not visible at position 3, can be detected. The amplitude of the Trp internal motions is significantly larger in this region of the protein than at position 3. The overall correlation time of the whole protein rotation is significantly smaller for the deleted mutant than for the undeleted one (Table VI).

Finally, despite the short mean excited-state lifetime exhibited by the Trp residue at position 94, the long correlation time of ~7.5 ns of the overall protein rotation contributes significantly to the anisotropy decay. A fast rotation is detected too, and the initial anisotropy value is around 0.245, close to the A_0 value at the excitation wavelength of 295 nm, indicating that no faster rotation is occurring at this position of the peptide chain. The wobbling angle is the largest observed for this series of mutants (Table V).

Effect of Calcium Binding on the Excited-State Lifetime Distribution and on the Rotational Mobility of Trp in Different Positions along the Peptide Chain. There is no significant effect of calcium binding to the wild-type protein, either on the emission maximum (Table III) or on the excited-state lifetime distribution of Trp-3 (Figure 2 and Table

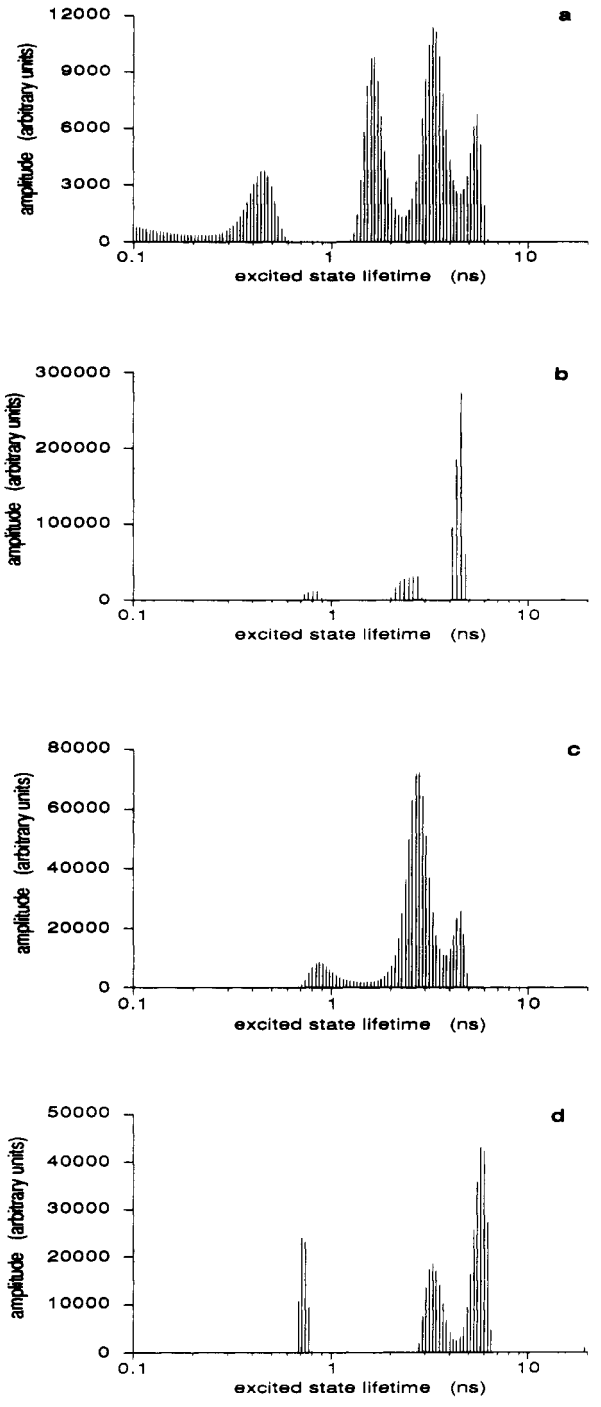

FIGURE 5: MEM-recovered excited-state lifetime distribution of the ΔW31 PLA_2 mutant: (a) unliganded protein; (b) protein in the presence of 50 mM $CaCl_2$; (c) protein in the presence of 50 mM $CaCl_2$ and 0.8 mM C12PN (monomeric form of the substrate analogue); (d) protein in the presence of 50 mM $CaCl_2$ and 4 mM C16PN (micellar form of the substrate analogue). The experimental conditions are described under Materials and Methods.

IV). The mobility of the indole ring is not changed either (Table V). In the case of the ΔW3 mutant, however, a change in the respective proportions of c_1 and c_3 is observed (Figure 3) (Table IV). However, no effect on the mobility can be observed (Table V).

The Trp-31 emission maximum in the W31 mutant is only slightly red-shifted upon calcium binding (~4 nm) (Table III). By contrast, a large increase (38%) in the quantum yield value is observed, parallel to an increase in the mean excited-state lifetime (Table IV). In the ΔW31 protein, the effect of calcium binding on the quantum yield is an 18% increase. The

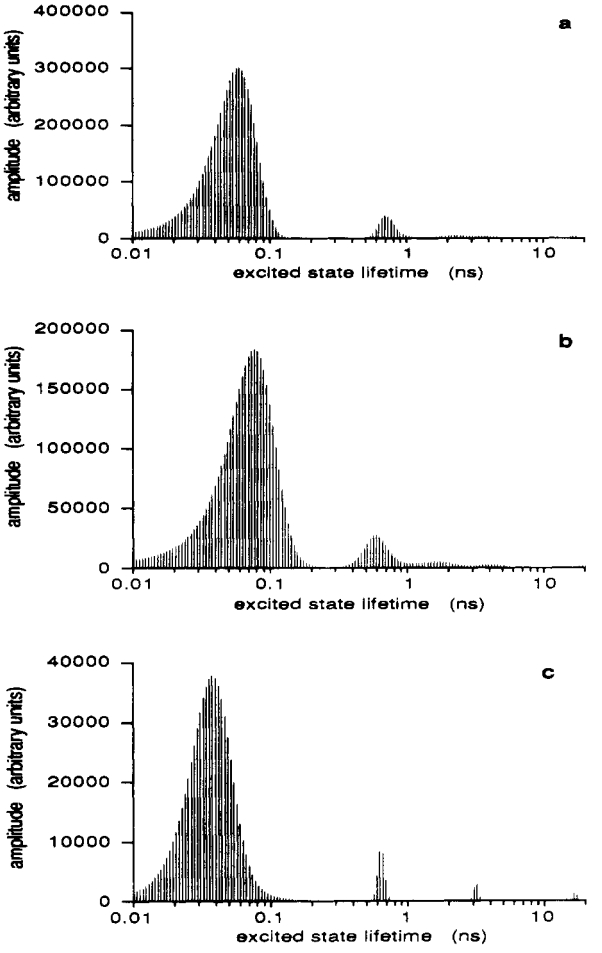

FIGURE 6: MEM-recovered excited-state lifetime distribution of the W94 PLA_2 mutant: (a) unliganded protein; (b) protein in the presence of 50 mM $CaCl_2$; (c) protein in the presence of 50 mM $CaCl_2$ and 4 mM C16PN (micellar form of the substrate analogue). The experimental conditions are described under Materials and Methods.

mean excited-state lifetime increases by 45%.

Time-resolved data showed that these average modifications mask large changes occurring on the excited-state lifetime distributions (Figures 4 and 5). The addition of calcium to the W31 protein dramatically decreases the two shortest lifetime contributions (Figure 4). As a result, ~80% of the decay can be accounted for by the two longest lifetimes components. The major changes concern the c_4 value (barycenter 5.5 ns), which increases from 13% in the absence of the Ca^{2+} ion to 50% in the W31 protein–calcium complex. The barycenter values of the contributing lifetime families are only slightly changed upon addition of calcium. The ΔW31 mutant exhibits some differences with respect to the undeleted W31 protein. Although the general trend of the effect of calcium ion binding on the 31-position is respected, i.e., the reduction of the number of excited-state populations, this effect is stronger since the number of excited-state lifetime classes decreases from 4 to 2, with 80% of the decay arising from the longest component (Figure 5). In contrast to results with the W31 protein, a decrease in the barycenter values is observed.

In agreement with the modifications of the excited-state population distribution, large effects of calcium binding on the protein flexibility are observed in the 31 region. Calcium addition strongly depresses the contribution of the long correlation time of the protein but increases that of the intermediate flexibility in the triple-exponential model (Table VI). The rate of this intermediate flexibility is decreased. A larger wobbling angle of rotation is calculated in the presence of the

Table VI: Effects of Ligand Binding on the Anisotropy Parameters of Trp-31 in PLA_2 Derivatives W31 and ΔW31[a]

enzyme	β_1	β_2	β_3	θ_1 (ns)	θ_2 (ns)	θ_3 (ns)	r_0	θ_{max}
W31		0.040 ± 0.004	0.170 ± 0.011[b]		0.7 ± 0.2	7.4 ± 0.3	0.210	34
	0.087 ± 0.036	0.039 ± 0.010	0.155 ± 0.012[c]	0.1 ± 0.08	1.7 ± 0.9	8.0 ± 0.7	0.281	30
+Ca^{2+}		0.056 ± 0.006	0.129 ± 0.007		0.8 ± 0.2	5.0 ± 0.5	0.185	43
	0.054 ± 0.026	0.084 ± 0.014	0.072 ± 0.014	0.4 ± 0.1	2.7 ± 0.3	6.8 ± 0.9	0.210	37
+C12PN (mono)		0.042 ± 0.003	0.169 ± 0.007		1.2 ± 0.3	6.50 ± 0.04	0.211	35
	0.016 ± 0.003	0.040 ± 0.001	0.165 ± 0.005	0.13 ± 0.03	1.5 ± 0.2	6.6 ± 0.1	0.221	28
+C12PN (micelle)		0.033 ± 0.001	0.156 ± 0.004		0.9 ± 0.1	12.4 ± 0.4	0.189	37
	0.075 ± 0.042	0.026 ± 0.00	0.153 ± 0.003	0.04 ± 0.00	1.4 ± 0.4	12.5 ± 0.1	0.254	33
+C16PN (micelle)		0.062 ± 0.035	0.185 ± 0.001		1.2 ± 0.1	24.4 ± 0.5	0.247	32
	0.033 ± 0.002	0.028 ± 0.001	0.182 ± 0.004	0.2 ± 0.1	1.4 ± 0.4	25.2 ± 0.7	0.243	28
ΔW31		0.052 ± 0.004	0.166 ± 0.002		0.6 ± 0.10	6.6 ± 0.2	0.218	35
	0.14 ± 0.16	0.039 ± 0.006	0.163 ± 0.003	0.16 ± 0.15	0.9 ± 0.1	6.7 ± 0.2	0.342	29
+Ca^{2+}		0.062 ± 0.009	0.131 ± 0.008		1.0 ± 0.3	6.1 ± 0.9	0.193	42
	0.051 ± 0.020	0.099 ± 0.014	0.073 ± 0.012	0.2 ± 0.1	2.6 ± 0.4	9.3 ± 2.2	0.223	34
+C12PN (mono)		0.036 ± 0.003	0.177 ± 0.003		0.6 ± 0.3	5.8 ± 0.7	0.216	33
	0.050 ± 0.028	0.045 ± 0.023	0.148 ± 0.024	0.2 ± 0.1	2.2 ± 1.0	6.5 ± 0.9	0.243	31
+C12PN (micelle)		0.041	0.156		1.3	13.6	0.197	37
	0.031	0.057	0.118	0.5	4.9	17.3	0.206	34
+C16PN (micelle)		0.039 ± 0.004	0.156 ± 0.015		1.1 ± 0.2	21.4 ± 2.5	0.195	37
	0.027 ± 0.015	0.028 ± 0.010	0.150 ± 0.009	0.4 ± 0.1	2.4 ± 0.9	23.0 ± 4.2	0.205	33

[a] The anisotropy decay was assumed as a sum of exponentials: $r(t) = \sum\beta_i \exp(-t/\theta_i)$. θ_{max} was calculated according to Kinosita et al. (1977). Excitation wavelength: 300 nm. Emission wavelength: 350 nm. [b] Biexponential model. [c] Triexponential model.

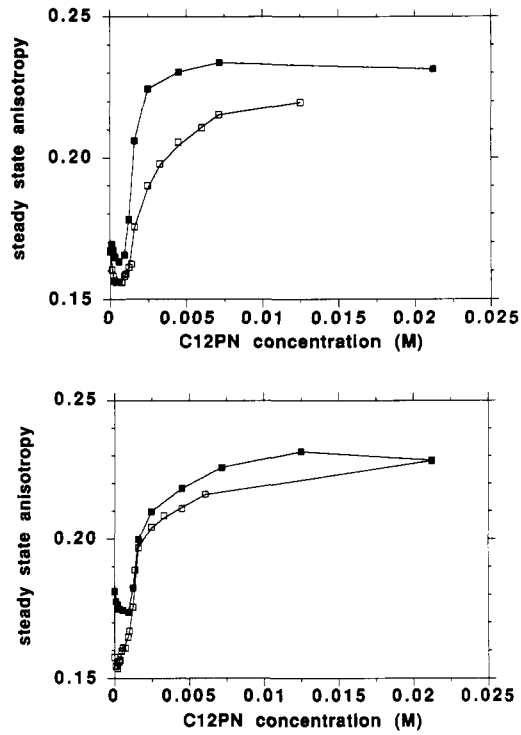

FIGURE 7: Variation of the steady-state anisotropy of Trp-3 in the wild-type PLA_2 protein (upper panel) and in the ΔW3 mutant (lower panel) as a function of C12PN concentration (■) without $CaCl_2$ and (□) in the presence of 50 mM $CaCl_2$. The temperature was 20 °C. Experimental conditions are described under Materials and Methods.

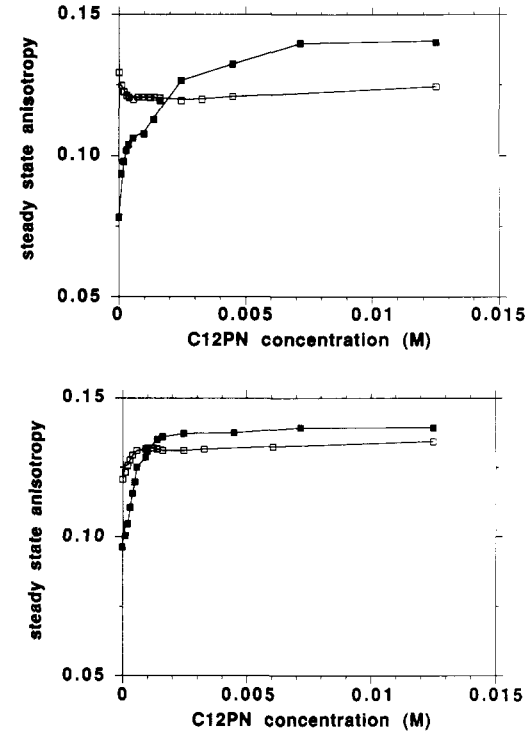

FIGURE 8: Variation of the steady-state anisotropy of Trp-31 in W31 PLA_2 (upper panel) and in the ΔW31 protein (lower panel) as a function of C12PN concentration (■) without $CaCl_2$ and (□) in the presence of 50 mM $CaCl_2$. The temperature was 20 °C. Experimental conditions are described under Materials and Methods.

ion (Table VI). One should note that the long correlation value is smaller for the W31 than for the ΔW31 protein–calcium complex.

No effect of experimental significance can be observed for the excited-state lifetime distribution of Trp at the 94-position (Figure 6).

Effect of Substrate Analogue Binding on the Fluorescence Characteristics of Trp in Different Positions along the Peptide Chain. The effect of monomer binding was first followed by measuring the variation of the steady-state anisotropy of the single Trp residue as a function of C12PN concentration (cmc = 1.3 mM). The measurements were performed in the absence and in the presence of calcium ions at 50 mM concentration, which is at least 20 times higher than the Ca^{2+} K_d. Since micelles are also formed with C12PN above 1.3 mM, their binding was also followed in this way.

In the W3 series, a small decrease of the steady-state anisotropy value is observed in the C12PN concentration range below the cmc (Figure 7). The decrease is more important in the absence of calcium ions. At concentrations above the cmc, the anisotropy value starts to increase. The enhancement is steeper in the presence of calcium, whereafter a plateau is reached. From these curves an estimate of around 70 C12PN molecules bound per protein molecule can be calculated. Similar behaviors are observed from the ΔW3 protein, although there is no large effect of the calcium ion.

In the W31 series (Figure 8), an effect is observed for the monomer binding whereas only a weak effect can be seen for

the micelle binding. Without calcium, the addition of C12PN to the W31 mutant solution leads to a decrease of the steady-state anisotropy value up to a concentration below the cmc, followed by a plateau. Upon addition of 50 mM calcium without any substrate analogue present, a large decrease of the steady-state anisotropy is observed in agreement with the increase in the mobility of Trp-31 observed in the time-resolved measurements described in the preceding paragraph. Addition of the substrate analogue reverses the effect: a two-step enhancement of the steady-state anisotropy is measured. The first rise occurs below the cmc and is due to the monomer binding, whereas the second rise is displayed at concentration above the cmc and is the result of micelle binding. In no case does the steady-state anisotropy value reach that observed for C12PN micelle binding to the W3 or ΔW3 mutants. For the ΔW31 mutant, a rise instead of a decrease in the steady-state anisotropy value is observed as a function of C12PN addition at concentrations below the cmc, without calcium. Addition of calcium ions without any substrate analogue present strongly decreases the steady-state anisotropy value but to a lesser extent than with the W31 mutant. This decrease is reversed by addition of C12PN.

More detailed information is provided by the time-resolved measurements. Small modifications of the lifetime distributions are displayed on Trp-3 upon interaction of the wild-type protein with monomers of C12PN (Figure 2). A decrease of the longest lifetime value and an enhancement of its contribution (c_4) at the expense of c_1 is observed. The excited-state lifetime distribution of the ΔW3 protein is similarly modified after C12PN monomer binding (Figure 3). Nevertheless, the decays of the complexes with the monomeric substrate analogue remain heterogeneous. C12PN monomer binding to the W3 proteins affects the Trp-3 internal motion to some extent, increasing slightly the amplitude of rotation (Table V).

In contrast to monomer binding, the interaction with C12PN micelles leads to a much more homogeneous fluorescence decay of Trp-3 (Table IV). In the case of the wild-type protein, the lifetime class with barycenter ~2.6 ns (which displayed a contribution of around 23% in the unliganded protein) represents 66% of the total intensity decay in the presence of the ligand. The effect is even more important for the C16PN micelle binding and the 2.6-ns class represents now 80–100% of the total intensity decay (Figure 2). The amplitude profile provided by MEM is broad (half-width = 1.1 ns). In the ΔW3–micelle complexes, the decays are more heterogeneous than in the wild-type–micelle complexes (see Figure 3 for the complex with C16PN). The major component remains the ~3-ns component (Table IV). In the protein complexes with micelles, a decrease of the amplitude of rotation of Trp-3 can be observed (Table V). In the case of the C16PN micelle–protein complex, the effects are stronger than with C12PN micelles: a reduction of the rate of internal motion and a large decrease in amplitude are observed (Table V).

Binding of C12PN monomers to the Trp-31 mutants leads to a further redistribution of the lifetime classes with respect to the situation in the presence of calcium ions. For the W31 mutant, the lifetime class with a barycenter of ~1 ns is suppressed, and the long-lifetime class (barycenter ~ 5 ns) then contributes to 73% of the decay (Figure 4). In the case of the complex of ΔW31 with a C12PN molecule, the redistribution of the excited-state populations affects those displaying the two longest lifetimes, which are difficult to separate (Figure 5) (Table IV). The internal motion of Trp-31 is affected by C12PN monomer binding (Table VI). The contribution of the nanosecond flexibility is depressed as compared to the situation in the presence of calcium only. A reduction of the wobbling angle of rotation with respect to the value in the presence of calcium ion is also found in both mutants (Table VI).

In the complex of W31 mutant with C12PN micelles, there are some changes in the lifetime distribution as compared to that in the Ca^{2+}–protein complex. Only an increase of the c_4 class and a parallel suppression of the c_1 class are observed (Table IV). The effect of C16PN binding is very similar (Figure 4). There is no significant effect on the barycenter values for the two longest lifetime classes (Table IV). For the ΔW31 protein, c_4 is increased upon C12PN micelle binding as compared to the protein–Ca^{2+} complex with C12PN monomer (Figure 5). The final lifetime distribution of the ΔW31–C16PN micelle complex is similar to the one displayed by the W31–C16PN complex (Table IV). The interactions of the W31 mutants with C12PN and C16PN micelles modify only slightly the Trp wobbling angle in the protein–micelle complexes, but the contribution of the nanosecond flexibility is decreased (Table VI).

For the W94–C16PN micelle complex, the short excited-state lifetime population remains dominant (Figure 6). An increase of the amplitude of motion is observed in the complex with C16PN micelles, and the rate of internal rotation is slowed down (Table V).

The values of the long correlation time of all the protein–micelle complexes are considerably enlarged with respect to the unliganded proteins. This results from the large increase in the size of the rotating body.

Discussion

Excited-State Lifetime Distribution and Mobility of the Tryptophan Residue at the Different Positions along the Peptide Chain of PLA_2. Because of the large set of possible interactions undergone by the Trp residue in proteins, its fluorescence intensity decay is rarely monoexponential [for example, see Grinvald and Steinberg (1976), Ross et al. (1981), Cockle and Szabo (1981), Beechem and Brand (1985), Nicot et al. (1985), Szabo et al. (1986), Szabo (1989), Gallay et al. (1987), Ludescher et al. (1985), Vincent et al. (1988), and Merola et al. (1989) for multiexponential decays, and Petrich et al. (1987), and James et al. (1985) for examples of monoexponential decays]. However, there is no general agreement about the molecular interpretation of this observation. The existence of an underlying quasicontinuum of thermally equilibrated excited-state populations generated by rates of exchange between the conformational substates of the order of magnitude of the excited-state decay rates has been suggested (James & Ware, 1985, 1986; James et al., 1987; Alcala et al., 1987a,b). In a second hypothesis, according to observations on tryptophan and derivatives in solution (Szabo & Rayner, 1980; Petrich et al., 1983; Chang et al., 1983; Engh et al., 1986; Colucci et al., 1990), a discrete series of conformations, produced by either slow exchange rates or jumps of the indole from one position to another one, are thought to occur within the protein matrix. However, it is likely that in one particular protein both situations held and that there exists a hierarchy of conformational substates (Frauenfelder et al., 1988). To develop methods able to discriminate between these extreme possibilities, with a minimum a priori assumption about the physical excited-state lifetime distribution, is of considerable interest.

In the case of excited-state lifetime determination by the time-correlated single-photon counting technique, the classical analysis by nonlinear least-squares regression postulates the existence of a discrete and limited series of excited-state

lifetimes. With the assumption of a correlation between the experiments, an improvement of the method by global analysis has opened the possibility to analyze more safely the data in terms of lifetime distributions (Willis et al., 1990). More recently, lifetime distributions have also been analyzed by a revised exponential series method (Siemarczuk et al., 1990). However, other methods able to handle a large set of exponential series can also be of great help to analyze fluorescence decay curves (Bajzer et al., 1990). The maximum entropy method has been proven to be a powerful tool when applied to fluorescence decay data (Livesey & Brochon, 1987). It can discriminate between discrete and continuous broad lifetime distributions in simulated curves (Vincent et al., 1988; Merola et al., 1989).

MEM analyses of the porcine PLA_2 fluorescence decays suggest the existence of separated well-defined classes of lifetimes for each derivative. The parameters of the quadruple-exponential model obtained by nonlinear least-squares regression analysis of the total fluorescence intensity decay data of the wild-type porcine PLA_2 (Ludescher et al., 1985) are in quite good agreement with the present ones after analysis by MEM. It then appears that the discrete lifetime values obtained by nonlinear least-squares regression reflect the barycenters of the underlying distribution for each lifetime class. A similar agreement between MEM and nonlinear least-squares analyses was also found in cases where both methods were used (Vincent et al., 1988; Merola et al., 1989; Gentin et al., 1990).

The fluorescence decay of the wild-type porcine pancreatic PLA_2 has also been investigated by the phase-modulation method (Alcala et al., 1987b). The results have been interpreted by different models: a discrete sum of exponentials (up to three) and unimodal and bimodal distributions of different shapes. On the basis of only a χ^2 criterion, with arbitrary chosen error bars, it appeared difficult to discriminate between these models. On the other hand, the temperature effect monitored in the referred paper indicated the existence of multiple potential wells for this protein. We suggest that this could well be represented by the four principal lifetime classes visualized after MEM analysis.

From the present set of data, the existence of separate classes of lifetimes for wild-type PLA_2 and its mutants is a likely possibility and argues against a continuous set of conformations. It precludes continuous distributions of conformational substates with exchanging rates of the order of magnitude of the excited-state duration. Instead, the tryptophan residue samples likely defined subconformations in slow exchange. The exchange rate values must be of an order of magnitude larger than the longest excited-state lifetimes (Engh et al., 1987). Alternatively, it is possible to envision fast jumps between conformations (Wahl, 1983). Such an interpretation is strengthened by the recently published studies on constrained tryptophan derivatives that show a close relationship between the excited-state lifetimes and the conformers in solution (Colucci et al., 1990).

The precise nature of the specific interactions leading to these lifetime classes is not straightforward to define. One observation is interesting: the respective barycenter values of each lifetime class in four porcine PLA_2 mutants (W3, ΔW3, W31, ΔW31) out of the five studied in this work are similar within a range of 10%. According to the crystallographic structure of the porcine PLA_2, Trp-3 stands at the protein surface exposed to water (Dijkstra et al., 1983). A similar exposition at the protein surface has been observed recently for the position 31 (Thunnissen et al., 1990). The values of the fluorescence emission maxima are in agreement with this picture. A working hypothesis could be that these typical lifetime values are characteristic of Trp residues located at the protein surface in contact with water, in a relatively polar environment. When the Trp residue is fully buried in a hydrophobic homogeneous environment, monoexponential decays with long-lifetime values can be observed (James et al., 1985; Petrich et al., 1987).

The residues closest to the Trp-3 position have been pointed in the crystal structure of the wild-type porcine PLA_2 (Dijkstra et al., 1983), with use of the MANOSK graphics program (Cherfils et al., 1988). Side chains of Ala-1, Leu-2, Gln-4, and Ser-72 are located within a sphere of radius 6 Å around the nitrogen atom of the indole ring. They are also inside a sphere of the same radius centered on carbon atoms situated on the same side of the indole ring as the nitrogen. Ser-7 is within a 6-Å distance for $C\epsilon 3$ and $C\zeta 3$ on the other side of the ring. Tyr-75 is within 6 Å distance from $C\zeta 3$. These residues are thus the closest neighbors of the Trp-3 indole ring and the most likely candidates for exchanging strong interactions. However, in the 6-Å sphere, eight water molecules are visible in the bovine enzyme, owing to the highest resolution (1.7 Å) of its crystal structure (Dijkstra et al., 1981). Interactions with water molecules of the hydration shell are likely also in the porcine enzyme.

The large similarity of the lifetime distributions of the W3 protein to that of the ΔW3 mutant in solution is in agreement with the resemblance of their crystal structures (Kuipers et al., 1989b). The conformations of the C_α chain and of the amino acid side chains in the N-terminal region, in particular that of the Trp-3, are highly conserved in both proteins. The closest residues within a sphere of a 6-Å radius are the same. However, due to the conformation change of the protein region close to the deleted loop, the Tyr-69 side chain is moved toward the surface of the molecule, and as a consequence its OH group is closer to the $N^{\epsilon}1$ of Trp-3 (Kuipers et al., 1989b). Ser-72 is also closer. These amino acids as well as those in the loop region do not appear therefore to influence the indole ring at position 3.

Similar interactions with the excited state are likely to occur for the Trp-31 residue, which is also exposed to the solvent as recently shown (Thunnissen et al., 1990). Therefore, water molecules are the most obvious common factor in the environment of both positions. The only exception for this similarly of environment is for the W94 mutant. The dominant interaction at this position is most probably occurring with the two proximate disulfide bridges (Cys-61/Cys-91 and Cys-51/Cys-98), which can act as powerful electron scavengers, resulting in a very efficient quenching (Steiner & Kirby, 1969).

By contrast to the similitude of the excited-state lifetime distributions, the internal mobility as observed by the fluorescence anisotropy decay of the Trp residue is quite different along the peptide chain. In the case of the natural position (W3 and ΔW3), a very short correlation time (≤100 ps), corresponding to the fast internal motion of the Trp-3 residue, occurs. A short correlation time with a large standard error was measured on the wild-type PLA_2 by Hudson's group, emphasizing the difficulty in determining accurately this short component, owing to its small value and to its low contribution (Ludescher et al., 1988). The wobbling angle of rotational motion calculated from the residual anisotropy (Kinosita et al., 1977) displays a relatively low value (~25–26°). From the examination of the crystal structure, the Trp-3 rotational motion around the C^α–C^β bond is not strongly hindered. Constraints on the rotation around the C^β–C^γ bond are

stronger, but nevertheless, the rotational freedom about this bond seems to be higher in the crystal than in solution. Recent simulation calculations have suggested that Trp-3 rotational motion is specifically hindered by interactions of the indole ring with water molecules (Axelsen et al., 1991), which could also be involved as mentioned in the excited-state interactions. A comparable situation is probably occurring for the ΔW3 mutant since our observations on this last protein are quite similar.

In opposition to these strongly restricted fast motions characterizing the N-terminal region, the calcium-binding loop region appears to be more flexible. In this region, the Trp-31 fluorescence anisotropy decay reveals a local flexibility that is absent in the N-terminal part of the protein in addition to very fast rotations, corresponding likely to deformation motions of the peptide segment bearing the Trp residue. A very similar situation is encountered for the ΔW31 mutant. The calculated wobbling angle displays higher values than at position 3. The higher flexibility of that part of the protein as compared to other regions was suggested by the temperature factor values in the crystal of the bovine enzyme (Dijkstra et al., 1981). Molecular dynamic trajectories calculations have also emphasized the higher flexibility of that part of the protein as compared to the N-terminal region (Sessions et al., 1988; Gros et al., 1990). These motions can favor the penetration of the substrate molecule into the active site cavity since the determined orientations of Tyr-69 and Leu-31 or Trp-31 in the mutant (Thunnissen et al., 1990), partially block the entrance to this cavity (Dijkstra et al., 1981, 1983; Kuipers et al., 1990b). It appeared from the calculations that an important part of the motion was due to backbone motion. It can be suggested that the fast subnanosecond depolarization motion detected in the present work is due to the rotation of the indole ring. The slower rotation can depict these backbone motions.

In the 94-position, the mobility of the Trp-94 residue appears to be of wider amplitude than that of Trp-3. Molecular dynamics trajectories calculations (Sessions et al., 1988) have suggested a concerted motion of helices C and E. However, these motions, involving extension and compression of the two helices, occur within an extremely short time scale (6 ps), questioning their relevance to the experimental observations.

The values of the long correlation times of all these proteins derived from the porcine pancreatic PLA_2, agree quite well with that measured in previous work on the wild-type protein (Ludescher et al., 1988). The molecule has the shape of a flattened ellipsoid with dimensions ~22 × 30 × 42 Å (Allegrini et al., 1985). The gyration radius is 13.7 Å, which corresponds to a volume of 1.07×10^4 Å^3. Calculation of the average rotational correlation time of the equivalent sphere of the same volume yields a value of 2.6 ns for the dry protein. If a hydration ratio of 0.4 g/g were assumed, a value of 4.9 ns would be calculated. The larger correlation time values that are measured in solution (7–8 ns) indicate that the shape of the rotating particle also has a large influence. According to the orientation of the Trp transition dipole with respect to these principal axes, the average correlation time can display different values, despite the fact that the fast internal mobility will average this orientation to some extent. The similar value observed for most of the mutants indicates a similar orientation of the indole transition dipole within the molecule, with respect to the ellipsoid axes.

Effect of Calcium Binding. The binding of calcium ions to the wild-type enzyme does not affect the Trp-3 excited-state lifetime distribution. The Trp-3 mobility is not affected either. An absence of a direct effect was expected, owing to the relatively large distance between the ion binding site and the Trp moiety (>10 Å).

In contrast, calcium ion modifies the distribution of Trp-31 conformers. It favors the excited-state population, displaying an excited-state lifetime value of ~5ns. This conformational substate preexisted in the unliganded protein but contributed to only ~10% of the different conformations. An even more homogeneous environment is found for the ΔW31 protein in the presence of calcium, further stressing the influence of the deleted loop 62–66 on the structure and dynamics of the calcium-binding loop. In agreement with the large effect on the excited-state population distribution, the mobility of the Trp-31 residue is strongly affected by calcium binding both in the W31 and in the ΔW31 mutants. A large increase of the wobbling angle of the fast motion of the indole ring and a strong enhancement of the contribution of the segmental flexibility are observed. These results are surprising since one would have expected that the two interactions involving the carbonyl groups of Gly-30 and Gly-32 with the calcium ion would have decreased the degrees of rotational freedom of the indole ring. The rotational correlation time associated to the segmental flexibility is, however, increased. A thorough reorganization in the peptide region bearing the Trp-31 residue is therefore mediated by calcium. Upon calcium binding to the carbonyl groups of Gly-30 and Gly-32, that part of the peptide chain could be shaped such that the indole is moved outside the loop, more in contact with the solvent. Such changes would explain the more homogeneous decay and the red shift of the fluorescence emission. In this conformation, the entrance to the active site cavity may be more accessible to the substrate since the flexibility of that peptide region is increased. This could explain in part the dependence of the catalytic activity for calcium ion. The recent X-ray structure of the ΔW31 protein complexed with calcium and a substrate analogue (Thunnissen et al., 1990) shows in fact that the indole ring is lying outside the calcium-binding loop.

Interactions with the Monomeric and Micellar Substrate Analogues. The interaction of the W3 and ΔW3 proteins with the monomeric substrate analogue C12PN affects the long-lifetime component in both its relative amplitude and its value that reveals that a specific but weak perturbation of the Trp-3 environment is induced by the presence of a single monoalkyl chain analogue. Slight perturbations of the mobility of the N-terminal region are visible. The slight decrease of the steady-state anisotropy value can be partially explained by the increase in the mean excited-state lifetime resulting from the increase of the long-lifetime class contribution. A small decrease in the rotational rate in the case of the wild-type protein and a moderate enhancement of the wobbling angle value for both proteins are also observed. These weak effects suggest that there is hardly any strong direct contact of the bound monomeric substrate molecule with Trp-3.

Much larger modifications of the Trp-3 excited-state lifetime distribution are displayed upon binding of the substrate analogue in micellar form in the case of either C12PN or C16PN than in the case of the C12PN monomeric substrate. Former results analyzed by nonlinear least-squares regression have also stressed the higher homogeneity of the Trp fluorescence decay in the complex of the protein with the micellar substrate analogue with respect to the unliganded protein (Ludescher et al., 1985). However, the present results, interpreted in the frame of the "conformer" hypothesis, definitely suggest that, in the complexes of the protein with the micelle, the indole ring is maintained in one major conformation. It was assumed that it became intercalated between the alkyl chains of the

substrate analogue, no more in contact with the protein moiety and the solvent (van Dam-Mieras et al., 1975). This hypothesis seemed to be substantiated by the large increase in the apparent quantum yield by about a factor 2.5–3 and the blue shift of the emission maximum of Trp-3 observed upon C16PN micelle binding (van Dam-Mieras et al., 1975; Ludescher et al., 1985). We shall remark that the reported quantum yield increase (van Dam-Mieras et al., 1975; Ludescher et al., 1985) overbalances that of the mean excited-state lifetime (×1.66). This difference can be explained by the increase in the absorbance at 300 nm of the tryptophan residue by a factor ~1.9 upon C16PN micelle binding (data not shown). Anyway, longer excited-state lifetime values would have been observed in the complexes if Trp-3 would be transferred to a hydrophobic medium (De Lauder & Wahl, 1971), which is not the case. An alternative interpretation for these steady-state fluorescence observations is provided by the time-resolved data. The blue shift of the emission spectrum such as mentioned in van Dam-Mieras's paper can be explained not only by a polarity effect but also by the selection of one particular conformer excited-state population emitting at a different wavelength corresponding to a microenvironment of lower polarizability, i.e., where interacting dipoles like peptide bonds or water molecules are immobilized by the micelle interface. It is to be pointed out that in this conformation the indole ring remains accessible to deuterated water (Jain et al., 1986). The anisotropy decay data support this hypothesis since the binding of the aggregated substrates C12PN and C16PN reduces the protein local flexibility as reported by Trp-3. It is likely that other groups of the protein and probably the water molecules are also immobilized in the complex.

In the ΔW3 protein, the conformational change induced by substrate aggregate binding reported by Trp-3 is similar to the above described effects on the wild-type protein, but two major conformations are coexisting in the C16PN–protein micellar complex. This may indicate a modified position of the inhibitor molecules in this complex with respect to that in the W3 protein. It is also possible that some of the hydrophobic residues in the loop itself (Phe-63 for instance) are involved in the micelle binding.

An important conformational change of the N-terminal part of the protein is therefore occurring upon substrate aggregate binding. If the interaction were analyzed in more details, the effect of the substrate analogue bearing the longest alkyl chain (C16PN) appears to be stronger than that of the shortest (C12PN). The differences in the structures and compositions of the protein–substrate complexes can be responsible for the observed effect. The aggregate of the wild-type protein with C16PN has been described to comprise two protein molecules and around 80 C16PN molecules (de Araujo et al., 1979), in good agreement with our results. The size of the complex of the wild-type protein with C12PN, estimated from the overall correlation time, appears definitely smaller with one protein molecule for 70 C12PN molecules. Furthermore, the packing of the alkyl chains in C16PN micelles is probably tighter than in C12PN micelles since, as it is generally accepted, the micelles of compounds with a low cmc are more densely packed than micelles of compounds with a low cmc.

The position 31 was in principle a better candidate than the position 3 to sense changes upon monomer binding because of its location at the entrance to the active site as already mentioned. The mobility of Trp-31 in both the W31 and ΔW31 mutants is in fact decreased in the monomer–protein complex with respect to that in the protein–calcium complex. This is especially observed in the triple-exponential model. This analysis shows that the peptide flexibility is reduced in amplitude as compared to that in the calcium–protein complexes as well as the wobbling angle. Despite these mobility changes, the excited-state lifetime distributions are not strongly affected. This last observation suggests that there are no strong direct contacts between the substrate analogue molecule and the indole. In the recently published tridimensional structure of the ΔW31 mutant complexed with a substrate analogue, no evidence of close contacts between these chains and the Trp-31 was obtained (Thunnissen et al., 1990).

In the W31 protein–micelle complexes either with C12 or C16PN, only slight modifications of the Trp-31 environment with respect to the calcium–protein complexes are noticeable. Only the contribution of the peptide flexibility is decreased. The perturbations of the Trp-31 environment by C12PN micelle binding seem to be more efficient in the ΔW31 than in the W31 proteins, but no difference is observable in the complexes of these two mutants with C16PN micelles. These small changes relative to the calcium effects were unexpected since position 31 belongs to the IRS. No direct contacts of the alkyl chains of C12PN or C16PN with Trp-31 and no large conformational changes seem therefore to occur in that part of the protein after binding to an interface. This protein region is therefore mainly stabilized by the binding of calcium.

In conclusion, specific and thorough modifications of the protein flexibility and structural heterogeneity are brought about by ligand binding to PLA_2. This evidences the structural adaptability of this protein. In order to produce the most efficient ternary complex for optimal catalysis, the protein structure must be specifically distorted from the crystallographic structure in specific areas like the N-terminal and the calcium-binding loop. In the N-terminal region, the flexibility of the protein is strongly reduced by interaction with the micelle interface and one major conformation is selected. This points to the need of a fixed conformation of this region to accommodate the micellar substrate. In contrast, the calcium binding enhances the flexibility of the peptide segment around the 31-position, thereby probably contributing to a better positioning of the substrate molecule.

ACKNOWLEDGMENTS

We thank the technical staff of LURE for running the synchrotron machine during the beam-time sessions. O.P.K. was supported by a short-term fellowship of the European Molecular Biology Organization. We are grateful to Will Botermans for technical assistance.

Registry No. C12PN, 29557-51-5; C16PN, 58066-85-6; diC6-dithioPC, 70504-26-6; diC8-PC, 19191-91-4; Ca^{2+}, 7440-70-2; phospholipase A_2, 9001-84-7.

REFERENCES

Alcala, J. R., Gratton, E., & Prendergast, F. G. (1987a) *Biophys. J. 51*, 597–604.

Alcala, J. R., Gratton, E., & Prendergast, F. G. (1987b) *Biophys. J. 51*, 925–936.

Axelsen, P. H., & Prendergast, F. G. (1989) *Biophys. J. 56*, 43–66.

Axelsen, P. H., Haydock, C., & Prendergast, F. G. (1988) *Biophys. J. 54*, 249–258.

Axelsen, H. P., Gratton, E., & Prendergast, F. G. (1991) *Biochemistry 30*, 1173–1179.

Bajzer, Z., Sharp, J. C., Sedarous, S. S., & Prendergast, F. G. (1990) *Eur. J. Biophys. 18*, 101–115.

Beechem, J. M., & Brand, L. (1985) *Annu. Rev. Biochem. 54*, 43–71.

Brunie, S., Bolin, J., Gewirth, D., & Sigler, P. B. (1985) *J. Biol. Chem. 260*, 9742–9749.
Bucci, E., & Steiner, R. F. (1988) *Biophys. Chem. 30*, 199–224.
Careri, G., Fasella, P., & Gratton, E. (1979) *Annu. Rev. Biophys. Bioeng. 8*, 69–97.
Change, M. C., Petrich, J. W., Mc Donald, D. B., & Fleming, G. R. (1983) *J. Am. Chem. Soc. 105*, 3819–3824.
Cherfils, J., Vaney, M. C., Morize, I., Surcouf, E., Colloc'h, N., & Mornon, J. P. (1988) *J. Mol. Graphics 6*, 155–160.
Cockle, S. A., & Szabo, A. G. (1981) *Photochem. Photobiol. 34*, 23–27.
Colucci, W. J., Tilstra, L., Sattler, M. C., Fronczek, F. R., & Barkley, M. D. (1990) *J. Am. Chem. Soc. 112*, 9182–9190.
Creed, D. (1984) *Photochem. Photobiol. 39*, 537–562.
Datema, K. P., Visser, A. J. W. G., van Hoek, A., Wolfs, C. J. A. M., Spruijt, R. B., & Hemminga, M. (1987) *Biochemistry 26*, 6145–6152.
de Araujo, P. S., Rosseneu, M. Y., Kremer, J. M. H., van Zoelen, E. J. J., & de Haas, G. H. (1979) *Biochemistry 18*, 580–586.
De Haas, G. H., Mulder, I., & van Deenen, L. L. M. (1960) *Biochem. Biophys. Res. Commun. 3*, 287–291.
De Lauder, W. B., & Wahl, Ph. (1971) *Biochim. Biophys. Acta 243*, 153–163.
Demaret, J. Ph., & Brunie, S. (1990) *Protein Eng. 4*, 163–170.
Dijkstra, B. W., Kalk, K. H., Hol, W. G. J., & Drenth, J. (1981) *J. Mol. Biol. 147*, 97–123.
Dijkstra, B. W., Renetseder, R., Kalk, K. H., Hol, W. G. J., & Drenth, J. (1983) *J. Mol. Biol. 168*, 163–179.
Engh, R. A. L., Chen, X.-Q., & Fleming, G. R. (1986) *Chem. Phys. Lett. 126*, 365–372.
Frauenfelder, H., Parak, F., & Young, R. D. (1988) *Annu. Rev. Biophys. Biophys. Chem. 17*, 451–479.
Gallay, J., Vincent, M., Nicot, C., & Waks, M. (1987) *Biochemistry 26*, 5738–5747.
Gentin, M., Vincent, M., Brochon, J. C., Livesey, A. K., Cittanova, N., & Gallay, J. (1990) *Biochemistry 29*, 10405–10412.
Grinvald, A., & Steinberg, I. Z. (1976) *Biochim. Biophys. Acta 427*, 663–678.
Gros, P., van Gunsteren, W. F., & Hol, W. G. J. (1990) *Science 249*, 1149–1152.
Henry, E. R., & Hochstrasser, R. M. (1987) *Proc. Natl. Acad. Sci. U.S.A. 84*, 6142–6146.
Ichiye, T., & Karplus, M. (1983) *Biochemistry 22*, 2884–2893.
Jain, M. K., Maliwal, B. P., de Haas, G. H., & Slotboom, A. J. (1986) *Biochim. Biophys. Acta 860*, 448–461.
James, D. R., & Ware, W. R. (1985) *Chem. Phys. Lett. 120*, 450–454.
James, D. R., & Ware, W. R. (1986) *Chem. Phys. Lett. 126*, 7–11.
James, D. R., Demmer, D. R., Steer, R. P., & Verall, D. E. (1985) *Biochemistry 24*, 5517–5526.
James, D. R., Turnbull, J. R., Wagner, B. D., Ware, W. R., & Petersen, N. O. (1987) *Biochemistry 26*, 6272–6277.
Jaynes, E. T. (1983) *Papers on Probability Statistics & Statistical Physics* (Rosenkrantz, R. D., Ed.) D. Reidel, Dordrecht.
John, E., & Jähnig, F. (1988) *Biophys. J. 54*, 817–827.
Karplus, M., & McCammon, J. A. (1981) *CRC Crit. Rev. Biochem. 9*, 293–357.
Kinosita, J., Jr., Kawato, S., & Ikegami, A. (1977) *Biophys. J. 20*, 289–305.
Kuipers, O. P., Dijkman, R., Pals, C. E. G. M., Verheij, H. M., & de Haas, G. H. (1989a) *Protein Eng. 2*, 467–471.
Kuipers, O. P., Thunnissen, M. M. G., de Geus, P., Dijkstra, B. W., Drenth, J., Verheij, H. M., & de Haas, G. H. (1989b) *Science 244*, 82–85.
Kuipers, O. P., Kerver, J., van Meersbergen, J., Vis, R., Dijkman, R., Vereheij, H. M., & de Haas, G. H. (1990a) *Protein Eng. 3*, 599–603.
Kuipers, O. P., Vincent, M., Brochon, J. C., Verheij, H. M., de Haas, G. H., & Gallay, J. (1990b) *SPIE Proc. 1024*, 10–111.
Lipari, G., & Szabo, A. (1980) *Biophys. J. 30*, 486–506.
Livesey, A. K., & Skilling, J. (1985) *Acta Crystallogr. A41*, 113–122.
Livesey, A. K., & Brochon, J. C. (1987) *Biophys. J. 52*, 693–706.
Ludescher, R. D., Volwerk, J. J., de Haas, G. H., & Hudson, B. (1985) *Biochemistry 24*, 7240–7249.
Ludescher, R. D., Johnson, I. D., Volwerk, J. J., de Haas, G. H., Jost, P., & Hudson, B. (1988) *Biochemistry 27*, 6618–6628.
MacKerell, A. D., Jr., Nilsson, L., & Rigler, R. (1988) *Biochemistry 27*, 4547–4556.
McCammon, J. A., & Harvey, S. C. (1987) *Dynamics of Proteins and Nucleic Acids*, Cambridge University Press, Cambridge.
Merola, F., Rigler, R., Holmgren, A., & Brochon, J. C. (1989) *Biochemistry 28*, 3383–3398.
Munro, I., Pecht, I., & Stryer, L. (1979) *Proc. Natl. Acad. Sci. U.S.A. 76*, 56–60.
Nicot, C., Vacher, M., Vincent, M., Gallay, J., & Waks, M. (1985) *Biochemistry 24*, 7024–7032.
Petrich, J. W., Chang, M. C., McDonald, D. B., & Fleming, G. R. (1983) *J. Am. Chem. Soc. 150*, 3824–3832.
Petrich, J. W., Longworth, J. W., & Fleming, G. R. (1987) *Biochemistry 26*, 2711–2722.
Pieterson, W. A., Vidaj, J. C., Volwerk, J. J., & de Haas, G. H. (1974) *Biochemistry 14*, 5394–5399.
Ross, J. B. A., Rousslang, K. W., & Brand, L. (1981) *Biochemistry 20*, 4361–4369.
Scott, D. L., White, S. P., Otwinowski, Z., Yuan, W., Gelb, M., & Sigler, P. B. (1990a) *Science 250*, 1541–1546.
Scott, D. L., Otwinowski, Z., Gelb, M., & Sigler, P. B. (1990b) *Science 250*, 1563–1566.
Sessions, R. B., Dauber-Osguthorpe, P., & Osguthorpe, D. J. (1988) *J. Mol. Biol. 209*, 617–633.
Siemiarczuk, A., Wagner, B. D., & Ware, W. R. (1990) *J. Phys. Chem. 94*, 1661–1666.
Slotboom, A. J., & de Haas, G. H. (1975) *Biochemistry 14*, 5394–5399.
Small, E. W., & Anderson, S. R. (1988) *Biochemistry 27*, 419–428.
Steiner, R. F., & Kirby, E. P. (1969) *J. Phys. Chem. 73*, 4130–4135.
Szabo, A. G. (1989) in *The Enzyme Catalysis Process* (Cooper, A., Houben, J. L., Chien, L. C., Eds.) pp 123–139, Plenum, New York.
Szabo, A. G., & Rayner, D. M. (1980) *J. Am. Chem. Soc. 102*, 554–563.
Sazbo, A. G., Krajkarski, D. T., Cavatorta, P., Masotti, L., & Barcellona, M. L. (1986) *Photochem. Photobiol. 44*, 143–150.
Thunnissen, M. M. G. M., Eiso, A. B., Kalk, K. H., Drenth, J., Dijkstra, B. W., Kuipers, O. P., Dijkmann, R., de Haas, G. H., & Verheij, H. M. (1990) *Nature 347*, 689–691.

Valeur, B., & Weber, G. (1977) *Photochem. Photobiol. 25*, 441-444.
van Dam-Mieras, M. C. E., Slotboom, A. J., Pieterson, W. A., & de Haas, G. H. (1975) *Biochemistry 14*, 5387-5393.
Verheij, H. M., Slotboom, A. J., & de Haas, G. H. (1981) *Rev. Physiol., Biochem., Pharmacol. 91*, 91-203.
Vincent, M., Brochon, J. C., Merola, F., Jordi, W., & Gallay, J. (1988) *Biochemistry 27*, 8752-8761.
Volwerk, J. J., & de Haas, G. H. (1982) *Lipid-Protein Interactions*, Vol. I, pp 69-149, Wiley-Interscience, New-York.
Volwerk, J. J., Dedieu, A. G. R., Verheij, H. M., Dijkman, R., & de Haas, G. H. (1979) *Recl. Trav. Chim. Pays-Bas 98*, 214-220.
Wahl, Ph. (1979) *Biophys. Chem. 10*, 91-104.
Wahl, Ph. (1983) in *Time-Resolved Spectroscopy in Biochemistry & Biology* (Cundall, R. B., & Dale, R. E., Eds.) NATO Advanced Science Institutes Series A: Life Sciences, Vol. 69, pp 497-522, Plenum Press, New York and London.
Waite, M. (1987) *The Phospholipases, Handbook of Lipid Research*, Vol. 5, Plenum Press, New York.
Werner, T. C., & Forster, L. S. (1979) *Photochem. Photobiol. 29*, 905-914.
White, S. P., Scott, D. L., Otwinowski, Z., Gelb, M. H., & Sigler, P. B. (1990) *Science 250*, 1560-1563.
Willis, K. J., Szabo, A. G., Zuker, M., Ridgeway, J. M., & Alpert, B. (1990) *Biochemistry 29*, 5270-5275.

How Accurately Can Oligonucleotide Structures Be Determined from the Hybrid Relaxation Rate Matrix/NOESY Distance Restrained Molecular Dynamics Approach?†

Kumaralal Kaluarachchi, Robert P. Meadows, and David G. Gorenstein*
Department of Chemistry, Purdue University, West Lafayette, Indiana 47907
Received March 8, 1991; Revised Manuscript Received June 26, 1991

ABSTRACT: The accuracy and precision of structures derived from a combined hybrid relaxation rate matrix/NOESY distance restrained molecular dynamics methodology were examined with simulations that included typical experimental errors. NOESY data were simulated for a DNA dodecamer duplex, d-$(CGCGAATTCGCG)_2$, with added volume error of ~20% and low-level thermal noise. Distances derived from a hybrid relaxation matrix analysis of the NOE data were used as constraints in molecular dynamics driven structural refinements of several initial model geometries. The final structures were compared against results obtained from the traditional isolated two-spin approximation treatment of these NOESY volumes and also against refined structures that employed error-free data. Results show that the structures derived from the relaxation rate matrix analysis of the NOESY data are more accurate than those derived from a simple two-spin approximation analysis and it is possible to achieve refinement to the level of simulated experimental error. Results may be significantly improved with the use of either more accurately measured NOESY volumes or additional matrix-derived constraints. Many of the helical parameters and backbone torsional angles may be accurately reproduced by the hybrid matrix methodology.

Of the currently available techniques for structural elucidation, only nuclear magnetic resonance (NMR) and X-ray crystallography allow one to observe the often subtle variations in DNA topology. Many fine reviews of the NMR method provide specific details and historical perspective (Hosur et al., 1988; Kearns, 1984; Patel et al., 1987b; Reid, 1987; Van De Ven & Hilbers, 1988). Briefly, the NMR method relies upon the use of the two-dimensional nuclear Overhauser effect (NOESY) to produce a set of interproton distance constraints that are used to refine model geometries (Broido et al., 1984; Feigon et al., 1983; Frechet et al., 1983; Gorenstein et al., 1990; Hare et al., 1983; Kearns, 1984; Scheek et al., 1984; Schroeder et al., 1987). Refinement methods are varied but have included distance geometry (Havel et al., 1983) and restrained molecular dynamics (Clore et al., 1985a,b, Gorenstein et al., 1990; Kaptein et al., 1985). While NMR spectroscopy has been largely successful in defining overall conformation as well as some sequence-specific variations in the local conformation of DNA (Assa-Munt & Kearns, 1984; Clore et al., 1985a,b; Gorenstein et al., 1988; Lefevre et al., 1987; Nilges et al., 1987; Patel & Shapiro, 1987; Patel et al., 1987a; Rinkel et al., 1987), several studies show disagreement between structures derived from X-ray crystallography and NMR-derived solution conformations (Joshua-Tor et al., 1988; Nikonowicz et al., 1990; Rinkel et al., 1987; Sklenâr & Bax, 1987). For example, a ^1H NMR study of a duplex decamer failed to reproduce sequence-specific variations in the sugar ring conformation predicted by X-ray crystal analysis (Rinkel et al., 1987); similar differences have been found in the backbone torsional angles (Sklenâr & Bax, 1987). The discrepancy between solution NMR structures and crystallographic X-ray structures raises the question whether the sequence-specific structural variations observed in the X-ray crystallographic studies are the result of packing forces. Indeed, variations in the local conformation may be found in different crystalline forms of the same duplex (Jain & Sundaralingam, 1989; Shakked et

†Supported by the NIH (AI27744), the Purdue University Biochemical Magnetic Resonance Laboratory, which is supported by the NSF National Biological Facilities Center on Biomolecular NMR, Structure and Design at Purdue (Grants BBS 8614177 and DIR-9000360 from the Division of Biological Instrumentation), and the National AIDS Research Center at Purdue (AI727713).

0006-2960/91/0430-8785$02.50/0